AN ABSTRACT OF THE THESIS OF

Alex Coyle for the degree of Master of Science in Civil Engineering presented on October 6, 2017.

Title: The Effects of Temperature on Electrical Resistivity Measurements of Concrete.

Abstract approved:

_____

W. Jason Weiss

Measuring resistivity as a method to calculate formation factor is becoming a popular way to evaluate transport properties of concrete. Resistivity measurements are dependent on multiple factors including the resistivity of the pore solution, leaching effects, the degree of saturation of the specimen, the age of the specimen (degree of reaction), the microstructural properties of the pore network (porosity and pore connectivity), and temperature. Temperature affects the bulk resistivity measurements of concrete specimens by changing the mobility of the ions in the pore solution. In addition to multiple fitting equations and temperature corrections, numerous values for temperature correction parameters have been proposed for a wide range of materials (i.e., solutions, pastes, mortars, and concretes at different degrees of saturation). In this study, a linear approach (using an α temperature coefficient) and an activation energy type approach (using an $E_{a\text{-}cond}$ temperature coefficient) are examined. These approaches were compared with each other numerically and their predictive capabilities were studied using measured resistivity data from several concrete mixtures. An equation is developed to convert a linear correction (α) to an activation energy type correction, ($E_{a\text{-}cond}$), given the testing temperature. Using a linear approach might be suitable for solutions and for saturated concrete, which have low values of α and $E_{a\text{-}cond}$. However, the use of $E_{a\text{-}cond}$ provides better predictive capabilities in sealed concretes, which have higher values of α and

$E_{a\text{-}cond}$, especially at low temperatures. An analysis of literature reveals that $E_{a\text{-}cond}$ values vary from 9 to 39 kJ/mol, for pore solutions, pastes, mortars and concretes with a variety of saturation states. In order to select an appropriate $E_{a\text{-}cond}$ for a specific specimen type, it is important to understand the factors affecting $E_{a\text{-}cond}$ of cementitious materials. $E_{a\text{-}cond}$ increases as degree of saturation of the specimen is reduced with a minimum $E_{a\text{-}cond}$ when the specimen is saturated. This is not due to the dilution of the pore solution, as pore solutions with different ionic strengths have similar $E_{a\text{-}cond}$. Rather, the increase of $E_{a\text{-}cond}$ upon drying is because of a change in the connectivity of the fluid filled pores. Under certain circumstances, changes in ionic mobility caused by changes in viscosity, may also affect $E_{a\text{-}cond}$. While it is better to directly measure the $E_{a\text{-}cond}$ of every concrete mixture, this is not always feasible. In such cases, for pore solutions a value of 13.9 kJ/mol can be used, for saturated concretes a value of 15.8 kJ/mol can be used and for sealed concretes a value of 29.8 kJ/mol can be used. For concretes with a varying degree of saturation, the $E_{a\text{-}cond}$ can be estimated if the degree of saturation (DOS) is known using the equation: $E_{a\text{-}cond} = 33.3 – 16.3 \cdot DOS$.

The Effects of Temperature on Electrical Resistivity Measurements of Concrete.

by
Alex Coyle

A THESIS

submitted to

Oregon State University

in partial fulfillment of
the requirements for the
degree of

Master of Science

Presented October 6, 2017
Commencement June 2018

Master of Science thesis of Alex Coyle presented on October 6, 2017

APPROVED:

Major Professor, representing Civil Engineering

Head of the School of Civil and Construction Engineering

Dean of the Graduate School

I understand that my thesis will become part of the permanent collection of Oregon State University libraries. My signature below authorizes release of my thesis to any reader upon request.

Alex Coyle, Author

ACKNOWLEDGEMENTS

I would like to offer my sincere appreciation towards Prof. Jason Weiss and our time spent together throughout my studies. His wisdom in his field of work and his ability to convey information clearly are qualities to aspire to.

I would also like to express my thanks to Robert Spragg who has bestowed upon me his knowledge of resistivity measurements of concrete, for helping me make sense of data, and the time helping clean Graf 100.

I would like to thank Prannoy Suraneni who has taken me under his wing as an academic and has given me lots of insight and has kept me focused and motivated.

I would like to thank Armen Amirkhanian for his technical wisdom and support as well as the insight he has given me.

I would like to thank Cameron Wilson, my friend and confidant across states and Luca Montanari for showing me how to make pasta while conjecturing and deliberating all aspects of life including work.

I would also like to thank my colleges: Chunyu Qiao, Marisol Tsui Chang, Cody Tibbits, Tengfei Fu, Mehdi Khanzadeh Moradllo, all of whom I continue to learn from.

I would like to thank the National Concrete Consortium and the Performance Engineered Mixtures (PEM) Champion States for funding these projects.

CONTRIBUTION OF AUTHORS

Jason Weiss, advisor, Robert Spragg, Armen Amirkhanian, and Prannoy Suraneni, post-doctoral researchers, were involved in the writing of Chapter 2.

Jason Weiss, advisor, Robert Spragg, Prannoy Suraneni, and Armen Amirkhanian, post-doctoral researchers, were involved in the writing of Chapter 3.

TABLE OF CONTENTS

Page

TABLE OF CONTENTS (Continued)

Page

LIST OF FIGURES

LIST OF TABLES

LIST OF ABBREVIATIONS AND VARIABLES

Abbreviation	Full Name	Description / Unit of Measure
a	Stokes radius of ion	Å
Å	Angstrom	10^{-10} m
AASHTO	American Association of State Highway and Transportation Officials	Organization
ASTM	American Society for Testing and Materials	Organization
$Ca(OH)_2$	Calcium hydroxide	Chemical
COV	Coefficient of Variation	%
DOS	Degree of saturation	Unitless
$E_{a\text{-}cond}$	Activation Energy of Conduction	kJ/mol
$E_{a\text{-}visc}$	Activation Energy of Viscosity	kJ/mol
F	Formation Factor	Unitless
FA	Fly ash	Material
HPC	High performance concrete	Material
K	Potassium	Chemical
KOH	Potassium hydroxide	Chemical
L	Liter	L
m_i	Initial mass of specimen	g
m_{od}	Mass of oven dried specimen	g
mol	Mole	mol
mol/L	Moles per liter	mol/L
m_{sat}	Mass of specimen after vacuum saturation	g
Na	Sodium	Chemical
Na_2O	Sodium oxide	Chemical
NaOH	Sodium hydroxide	Chemical
OPC	Ordinary Portland Cement	Material
P	Pressure	Pa
PEM	Performance Engineered Mixtures	Material
R	Universal gas constant	J/mol•K
S	Slag	Material
T	Temperature of specimen	K
TER	Ternary blend	Material
Tref	Temperature at reference	K
w/cm	Water-to-cementitious material ratio	Mass fraction
XRF	X-ray fluorescence	Machine
α	Linear temperature correction	%/°C
β	Connectivity of pore network	Unitless
β'	Connectivity of fluid filled pore network	Unitless

η	Viscosity	Pa·s
ρ	Resistivity of specimen	Ohm-m
ρ_0	Resistivity of pore solution	Ohm-m
ϕ	Porosity of specimen	Unitless

1. Introduction

The construction industry has seen a push for high performance concrete (HPC) in the past 50 years. HPC is obtained using lower water-to-cementitious materials ratio (w/cm) along with various chemical admixtures to improve concrete properties. HPC is not only concrete with higher strength but also lower permeability and thus higher durability. Concrete with greater service life has become highly desirable in pavements and bridge decks, and for such applications, durability is perhaps more important than strength. As such, there is a need to provide adequate specification to describe the durability of concrete as a material property. The American Association of State Highway Transportation Officials (AASHTO) is currently developing a specification for concrete pavements bride decks which deals with several durability issues such as salt damage, freeze thaw damage, corrosion and volume change.

A number of durability issues are related to the transport properties of the concrete. As an example, the time to corrosion is largely influenced by the transport of chloride ions diffusing to the depth of the rebar. As such, the transport of chloride in the concrete may be studied using direct methods, such as chloride ponding testing (ASTM C1556). However, this method has some drawbacks - it is a very time-consuming process, and it is a destructive test meaning multiple specimens are needed (otherwise the results give only a snapshot of one specific sample at a specific age).

Electrical measurements are a good alternative to evaluate transport properties of concrete. Although electrical testing for concrete has been around for several

decades (*1–4*), rapid and accurate use for concrete testing is a relatively recent development (*5–7*).

A commonly used electrical test to assess chloride penetration resistance is the rapid chloride penetration test (RCPT). This is a standard test (ASTM C1202) and has generally been the main alternative to directly measuring chloride penetration. While the test is relatively quick and easy to perform, it has several issues associated with it (as an example from heating due to the Joule effect) (*8–10*). Therefore, other ionic diffusion tests (such as the SIMCO Stadium approach) (*11*) have also been developed.

Recently much work has been done on electrical resistivity measurements of concrete as they are a quick and rapid method to evaluate transport properties (*12*, *13*). In addition, they are accurate, with single laboratory variation reported between 3-6% and multi-laboratory variation reported as 6-17% (*14*). Resistivity can be measured using surface, bulk and embedded sensors (*15*) but needs to be corrected using geometry factors which can determined experimentally or numerically (*16–18*).

In addition to geometrical effects, other factors influence resistivity measurements. Differences in the resistivity of the pore solution have an effect of the bulk resistivity of the specimen (*19*). In addition, alkali leaching impacts the resistivity of the pore solution inside the specimen (*20*). Degree of saturation (*3*, *4*, *21*, *22*) and temperature (*23–25*) have been shown to effect the resistivity of concrete. The porosity and the connectivity of the pore network also affect the resistivity of concrete specimens (*26*).

Formation factor (F), obtained from resistivity measurements, has been proposed as a parameter to evaluate the microstructural and transport properties of concrete specimens. Formation factor is based on Archie's law (*27*) and is inversely proportional to the porosity and the connectivity of the pore network. Formation factor is calculated by dividing the bulk resistivity of the specimen by the resistivity of the pore solution (*28*). Formation factor is given by Eq. 1-1

$$F = \frac{\rho}{\rho_0} = \frac{1}{\phi\beta} \quad (1\text{-}1)$$

where ρ is the bulk resistivity of the specimen (Ohm-m), ρ_0 is the resistivity of the pore solution (Ohm-m), ϕ (unitless) is the porosity of the specimen, and β (unitless) is the connectivity of the pores.

When determining formation factor, the pore solution resistivity can be either assumed as 0.10 Ωm (*29*), calculated from the alkali content of the cementitious materials (*30*), or can be measured experimentally from extracted pore solution (*31*). Formation factor and RCPT are mathematically related, based on first principles, as the charge passed in RCPT is inversely related to the resistivity of the concrete (*18, 29*). Additionally, an apparent diffusion coefficient can be calculated from formation factor using the Nernst-Einstein equation (*29, 32*).

Formation factor can be used in the specification of concrete durability because it is independent of the resistivity and chemical composition of the pore solution (*28*). Although formation factor is typically measured for fully saturated systems, this saturation state is not representative of field conditions. Air voids are typically not saturated in the field whereas in vacuum saturated specimens, the air voids are also fluid-filled. It has thus been proposed that a sealed condition is

representative of a concrete with its capillary and chemical shrinkage pores filled (*32*). A formation factor for a sealed condition (which has been shown to be a repeatable saturation state (*33*)) is commonly specified (*29*) and is given by Eq. 1-2

$$\rho_{T_{ref}} = \rho_0 \cdot F \cdot f(DOS) \cdot f(T) \cdot f(Leach) \quad (1\text{-}2)$$

where $\rho_{T_{ref}}$ is the bulk resistivity at a room temperature (Ohm-m), ρ_0 is the resistivity of the pore solution (Ohm-m), F is the formation factor (unitless), $f(DOS)$ is the function to correct for saturation state, $f(T)$ is the function to correct for temperature, $f(Leach)$ is the function to correct for leaching.

This thesis focuses on the effect of temperature on resistivity measurements and the development of a correction protocol that can be used to accurately predict resistivity measurements of concrete specimens at different temperatures. The development of a temperature correction is essential for the implementation of formation factor and its use as a specification as temperatures can show considerable variation in the field.

Temperature affects resistivity by changing the kinetics of ionic transport in solution. The effects of temperature on electrical measurements have been studied in literature (*8*, *23–25*, *34–36*). Multiple corrections have been proposed, including a linear correction and an activation energy based correction. These corrections have parameters (α and $E_{a\text{-}cond}$ respectively) that describe how sensitive resistivity measurements are to temperature. Throughout literature a wide range of fitting parameters have been reported. These parameters have been reported for solutions, pastes, mortars, and concretes at varying moisture contents. There is a lack of consistency regarding the appropriate temperature correction and fitting parameter.

This thesis will provide guidance on selecting the appropriate temperature correction and in addition, explain the factors that affect these temperature corrections.

1.1 Research Objectives

The objectives of this study are:

- To review the wide range of temperature correction fitting parameters in literature and to compare these values to measured data;
- To compare linear and activation energy temperature corrections and to ensure the appropriate one is used;
- To provide an equation to convert a linear temperature correction to an activation energy based correction;
- To provide guidelines on the determination of the correct fitting parameter based on the material tested (i.e. pore solutions vs. concrete specimens) and saturation sate of that specimen (i.e. saturated vs. sealed);
- To provide guidelines on measurement of a temperature correction specific to a concrete mixture at a certain saturation state; and
- To understand the physical mechanisms that affect these fitting parameters;

1.2 Thesis Organization

This thesis is composed of four chapters consisting of an introduction, two journal articles, and a conclusion.

Chapter 1 is an introduction to the thesis and provides background to the topics discussed. The introduction describes the current state of electrical resistivity

measurements used to determine formation factor as an approach to evaluate service life. The introduction discusses the importance of electrical measurements and describes the factors influencing resistivity measurements (including temperature). The objectives of the study and the organization of the thesis are outlined in Chapter 1.

Chapter 2 contains the first article: Comparison of Linear Temperature Corrections and Activation Energy Temperature Corrections for Electrical Resistivity Measurements of Concrete. This article compares two approaches to temperature correction of resistivity commonly found in literature: a linear temperature correction approach and an activation energy correction approach. These approaches are compared to each other numerically as well as compared using measured experimental data.

Chapter 3 contains the second article: Factors Affecting Activation Energy of Conduction of Cementitious Materials. This article describes the factors affecting activation energy values for concretes and provides guidance on selecting appropriate values.

Chapter 4 presents the main conclusions from this thesis.

2. Comparison of Linear Temperature Corrections and Activation Energy Temperature Corrections for Electrical Resistivity Measurements of Concrete

2.1 Abstract

Electrical resistivity measurements are being increasingly used as measurements for concrete acceptance in practice. It has been shown that these measurements are sensitive to temperature. This paper examines the influence of temperature on electrical resistivity measurements in concrete. Two commonly used approaches for temperature corrections were evaluated: a linear temperature correction approach (α) and an activation energy based temperature correction approach ($E_{a\text{-}cond}$). These approaches were compared with each other and their predictive capabilities were assessed using measured data from various concrete mixtures. It was found that for cases of low temperature sensitivity, the predictions obtained with α and with $E_{a\text{-}cond}$ were very similar. However, the $E_{a\text{-}cond}$ approach was found to provide more accurate corrections than corrections using α for measurements conducted at lower temperatures and for systems with higher temperature sensitivities. For saturated concrete specimens, both the linear (α) and activation energy ($E_{a\text{-}cond}$) approaches are acceptable while the use of $E_{a\text{-}cond}$ approach provides better predictive capabilities in sealed concrete specimens, especially at low temperatures. Average values for $E_{a\text{-}cond}$ were found to be 29.8 kJ/mol for sealed specimens and 15.8 kJ/mol for saturated specimens, and corresponding average values of α are 3.25 %/°C and 2.00 %/°C, respectively. The saturated values are closer to what may be expected of a pore solution on its own.

2.2 Introduction

Electrical measurements are a convenient method to evaluate the transport properties of concrete (*5*, *6*, *37*). Electrical measurements are easy to perform and can be performed rapidly (*7*). As such these methods are becoming more widely used (*5*–*7*, *32*, *38*). Electrical measurements can be used to calculate formation factor, which is a material property describing the volume and connectivity of the pore network inside a porous material (*27*), and can be used to relate to the ionic transport properties, such as an effective diffusion coefficient (*32*, *33*, *39*). The resistivity of a porous medium with a single conductive phase consisting of ionic pore solution can be described by the modified parallel law shown in Eq. 2-1 (*40*).

$$\rho = \rho_0 \frac{1}{\phi\beta} = \rho_0 F \tag{2-1}$$

where ρ is the total bulk resistivity (Ωm), ρ_0 is the resistivity of the pore solution (Ωm), ϕ is the fluid filled porosity (unitless), β is the connectivity of the pores (unitless), and F is formation factor (unitless).

Electrical measurements of concrete specimens are dependent on factors such as temperature (*8*, *14*, *34*, *35*, *41*), sample geometry (*18*), degree of saturation (*3*, *22*, *32*, *33*), storage conditions (*14*, *20*, *42*), and ionic concentration of the pore solution (*32*, *43*, *44*).

Bulk resistivity measurements are affected by the temperature of the specimen as temperature changes the mobility of ions in the pore solution. Higher temperatures increase ionic mobility and result in a lower pore solution resistivity ρ_0. The effect of temperature on electrical measurements on concrete has been studied previously and different corrections have been proposed. In this study, a linear correction as shown

in Eq. 2-2 (*23*), and an activation energy based correction as shown in Eq. 2-3 (*24*, *35*) are examined.

$$\rho_{Tref} = \left(\rho_T \frac{\left(T - T_{ref}\right)\alpha}{100} + 1 \right) \quad (2\text{-}2)$$

$$\rho_{Tref} = \rho_T \exp\left[\frac{-E_{a-cond}}{R} \left(\frac{1}{T + 273} - \frac{1}{T_{ref} + 273} \right) \right] \quad (2\text{-}3)$$

where ρ_T and ρ_{Tref} are the resistivities of concrete (Ωm) at temperatures T (°C) and T_{ref} (usually 23°C) respectively, α (%/°C) is the linear coefficient, $E_{a\text{-}cond}$ (kJ/mol) is the activation energy of conduction, and R (8.314 J/(mol K)) is the universal gas constant. The fitting parameters α and $E_{a\text{-}cond}$ describe the temperature dependency of electrical measurements. Higher values of these parameters correspond to resistivity measurement being more sensitive to temperature.

2.3 Research Objectives

While several temperature corrections have been proposed in literature, a detailed 'head to head' comparison of these corrections has not been performed to the best of the authors' knowledge. Clarification on the temperature corrections is needed as specifications develop. In this study, temperature corrections are performed on a wide range of commercially produced concretes using both a linear correction and an activation energy approach. The first objective of this study is to compare the use of these two corrections. The second objective is to compare the predictions of these two approaches for measured data using both sealed and saturated concrete mixtures.

2.4 Materials

This study was conducted using specimens from a multi-laboratory study. The specimens were standard 102 x 203 mm (4 x 8 in) concrete cylinders that were cast at different locations across the United States. Each mixture represents a different pavement or bridge deck mixture design with the water-to-cementitious materials ratio (w/cm) ranging from 0.37 to 0.45. The mixture designs along with the equivalent alkali content of the cementitious materials are provided in Table 2-1.

Specimens were cast onsite and left in their cylinder molds then sealed by double bagging with two 6 mil (0.15 mm) plastic bags. After being received at the laboratory, they remained sealed until a total age of 180 days, an age chosen to be representative of mature concrete. Sealed curing was chosen to minimize alkali leaching, which can introduce complexities in understanding pore solution properties (*20*). Additionally, it is a curing conditioning that can be easily specified and achieved (*32*). After 180 days of sealed curing, the specimens were subjected to the testing program described in detail in the Experimental Techniques section.

Table 2-1 Mixture proportions of the concretes used in this study.

Mixture ID	w/cm	Water (kg/m^3)	Cement* (kg/m^3)	Fly Ash* (kg/m^3)	Slag* (kg/m^3)	Silica Fume* (kg/m^3)	Air (%)	Aggregate (kg/m^3)
OPC-1	0.42	141	335 [0.76]	-	-	-	6.5	1828
OPC-2	0.41	161	390 [1.09]	-	-	-	6.5	1738
1P-1[1]	0.40	135	335 [0.64]	-	-	-	7.3	1790
FA-1	0.39	122	248 [0.60]	62 [2.78]	-	-	6.8	1906
FA-2	0.37	154	332 [0.52]	82 [0.92]	-	-	5.0	1749
FA-3	0.44	143	279 [0.73]	43 [1.11]	-	-	7.0	1817
FA-4	0.42	142	273 [0.52]	68 [1.38]	-	-	6.5	1837
S-1	0.43	141	247 [0.58]	-	82 [0.83]	-	6.0	1820
1S-1[2]	0.40	131	262 [0.54]	66 [1.30]	-	-	6.0	1805
TER-1	0.43	136	205 [0.55]	47 [1.90]	65 [0.84]	-	5.5-8.0	1878
TER-2	0.39	151	249 [0.58]	98 [1.80]	39 [0.83]	-	5.5-8.0	1786
TER-3	0.30	169	366 [0.53]	113 [1.33]	85 [0.84]	-	8.7	1518
TER-4	0.42	145	263 [0.70]	-	69 [0.84]	15 [0.40]	9.2	1658

[1] denotes a 1P(25) cement (*45*)
[2] denotes a 1S(20) cement (*45*)
*The values in the square brackets denote the Na_2O equivalent alkali contents from mill certificates

2.5 Experimental Techniques

2.5.1 Measurement of Resistivity at Varying Temperatures

The concrete specimens were prepared for measurements by applying a conductive nickel coating to the top and bottom surfaces after first scarifying the surfaces with a 20 grit concrete sanding block to improve adhesion. The nickel coating forms an electrode on the sample as typically seen in uniaxial resistivity measurements (*46, 47*). The direct attachment of the electrode eliminated the need for

a saturated sponge and the associated effects of measurement uncertainty due to the sponge drying over time (*48*). The Giatec RCON2™ and the Proceq Resipod resistivity meters (in its uniaxial configuration) were used to measure the resistivities of the samples. Tests on selected concrete specimens revealed that the resistivity values measured using the two meters were nearly identical (less than 1% variation). Leads from the resistivity meter were attached to the coated ends of the cylinders with aluminum tape to ensure a consistent electrical connection. Additionally, the outer circumference of the specimen was wrapped with two layers of plastic to minimize moisture loss during the test. While monitoring the resistivity of the specimens, the temperature was cycled. A range of temperatures from 5°C to 30°C was selected as it represents a range at which the majority of field resistivity measurements are typically performed. Additionally, this temperature range ensures that freezing does not occur (*46*).

For sealed samples, temperature was controlled and changed using the thermoelectric cold plate shown in Figure 2-1a. The specimen was placed upright on top of a 3 mm thick, thermally conductive pad (ThermaCool TC3008) to provide a thermal connection. An insulated aluminum shell thermally connected to the cold plate was used to isolate the sample from the exterior environment and promote uniaxial heating and cooling. This setup is similar to that described in previous work (*46*).

To enable a greater number of samples to be tested simultaneously a cooling coil device was built to control the specimen temperatures of the saturated specimens. Figure 2-1b shows the apparatus used to cycle the temperature. It should be noted this

device can also be used for sealed specimens as well. The testing device consisted of copper cooling coils surrounding the concrete cylinders connected to a water bath to control and vary the temperature of the specimens. A thermistor with an accuracy of 0.1°C was embedded into an additional, well-hydrated, concrete cylinder that was used to quantify the representative temperature of all specimens. Six specimens were placed in the remaining coils where their temperature was lowered to 5°C. The temperature was then raised in 5°C increments. It took approximately 90 minutes for a typical specimen to reach uniform temperature. After the specimens were at a uniform temperature, the resistivities were measured, the temperature was increased, and the process was repeated. Although the two apparatuses have different mechanisms for cooling the samples, the temperature cycles the specimens undergo were identical.

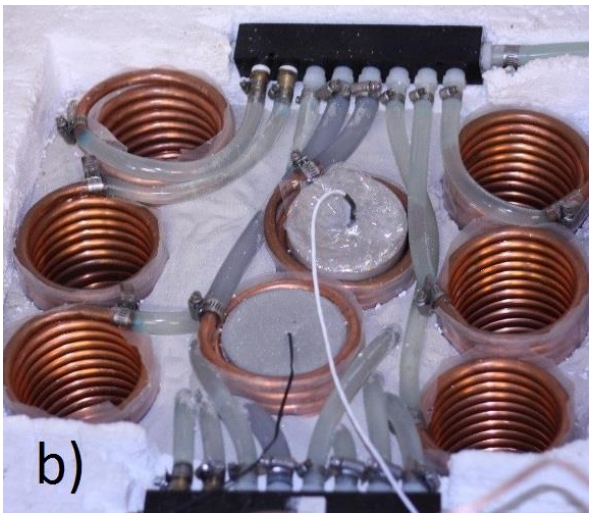

Figure 2-1 Temperature control apparatuses a) Cold plate, and b) Cooling coil.

2.5.2 Changing Concrete Degree of Saturation

The resistivities of the specimens in sealed conditions were measured at 180 days. It should be noted that the degree of saturation for sealed samples varies, depending on factors such as w/cm, paste content, and air content (*32*). To bring the samples to 100% degree of saturation the following approach was used. The mass of the sealed sample was measured. Specimens were then dried in a 110 ± 5°C oven until their mass equilibrated. They were then placed in a vacuum chamber with an absolute pressure of 10 ± 3 torr (1.33 ± 0.4 kPa) for three hours. While still under vacuum, deaerated saturated calcium hydroxide solution was added and specimens were soaked for one hour before removing from the vacuum chamber. The specimens remained under solution for an additional 24 hours before testing. This vacuum saturation procedure is outlined elsewhere (*49*).

2.6 Results and Discussion

2.6.1 Numerical Comparison of Temperature Corrections

The linear temperature correction (Eq. 2-2) and the activation energy correction (Eq. 2-3) can be numerically compared to each other by solving for ρ_{Tref}/ρ_T in Eq. 2-2 and 2-3 and setting them equal to each other resulting in Eq. 2-4

$$\alpha = \frac{\exp\left[\frac{-E_{a-cond}}{R}\left(\frac{1}{T+273}-\frac{1}{T_{ref}+273}\right)\right]-1}{\frac{\left(T-T_{ref}\right)}{100}} \qquad (2\text{-}4)$$

where $E_{a\text{-}cond}$ is the activation energy of conduction (kJ/mol); for the purpose of this analysis, $E_{a\text{-}cond}$ is a variable, ranging from 0-40 kJ/mol. T_{ref} is the reference temperature (23°C). T is the temperature at which resistivity is (theoretically) measured, it is a variable, ranging from 5-45°C. The relationship between these two corrections can be shown graphically (Figure 2-2) for five values of T.

The results show that in general as α increases the activation energy $E_{a\text{-}cond}$ increases. At low values of $E_{a\text{-}cond}$ (0-15 kJ/mol), a strong correlation exists between $E_{a\text{-}cond\ and}$ the value of α. For low values of $E_{a\text{-}cond}$, the relationship between $E_{a\text{-}cond}$ and α is relatively independent of T, and the two corrections have similar predictive capabilities. For high values of $E_{a\text{-}cond}$ (15-45 kJ/mol), the relationship between $E_{a\text{-}cond}$ and α is highly non linear with temperature (which ranges from approximately 2-9 %/°C) which increases as T increases. Therefore, there is not a unique relationship between $E_{a\text{-}cond}$ and α.

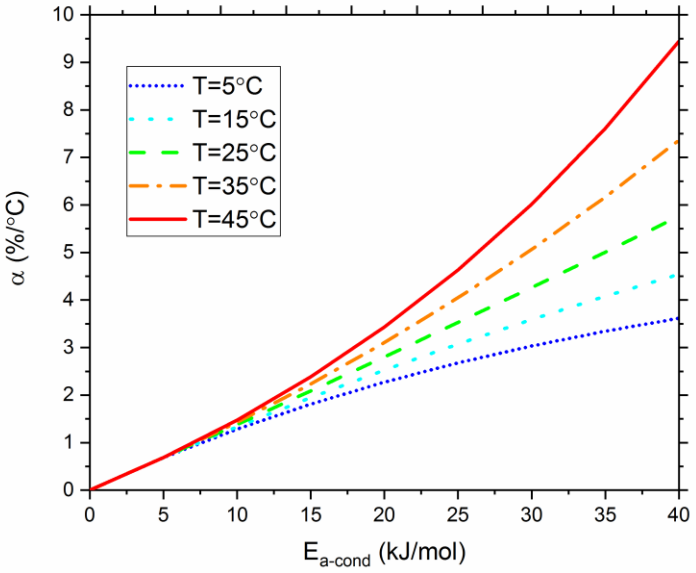

Figure 2-2 Comparison of $E_{a\text{-}cond}$ and α at different temperatures.

Throughout literature, a range of values of α have been reported for cementitious materials (*23*, *50*). Eq. 2-4 could be used to convert an α value to an $E_{a\text{-}cond}$ value so that the corrections may be compared. However, in order to do this accurately, the range of measured temperature should be taken into account.

Consider a scenario in which T_{ref} is 23°C and the $E_{a\text{-}cond}$ is 25 kJ/mol. For these conditions, an $E_{a\text{-}cond}$ of 25 kJ/mol corresponds to multiple values of α (2.68, 3.53, and 4.63 %/°C) depending on the second temperature T at which resistivity was measured (5, 25, 45°C). The comparison is illustrated in Figure 2-3a, 2-3b, and 2-3c respectively. These figures are obtained by plotting Eq. 2-3 and Eq. 2-2 as a function of temperature.

It is observed from Figure 2-3 that the absolute difference between the two corrections is relatively small (below 10%) between the theoretical temperature values used in Eq. 2-4. It should be noted that at temperatures outside this range, the

difference between the two corrections continually increases. It can also be noted from the figure that temperature corrections outside the range of values for which α was originally calculated should be considered with caution. This is especially true at lower temperatures where the increase in error is greater. In addition, at lower temperatures, the difference between the two corrections increases as α increases.

This is especially apparent in Figure 2-3c where the quantity $((T-T_{ref})\alpha)/(100)$ reaches a value of -1 and the equation yields an error. Based on Figure 2-3, one could state that $E_{a\text{-}cond}$ is a more stable temperature correction compared to α.

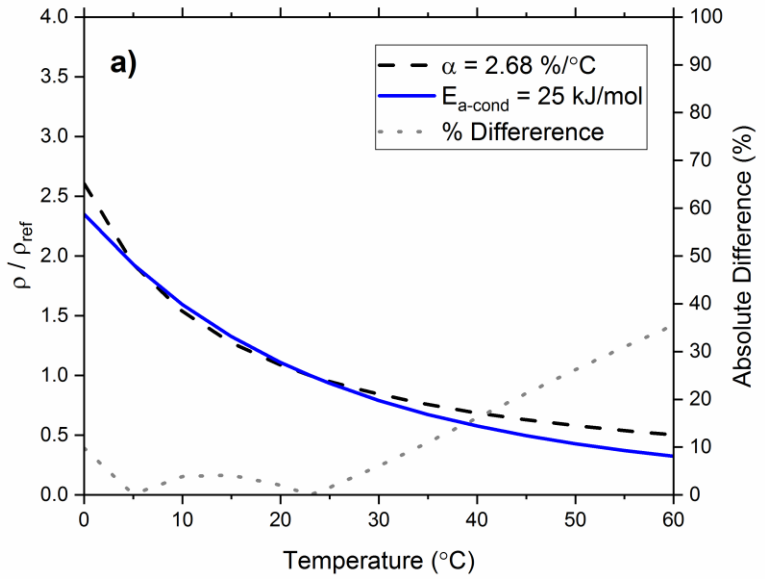

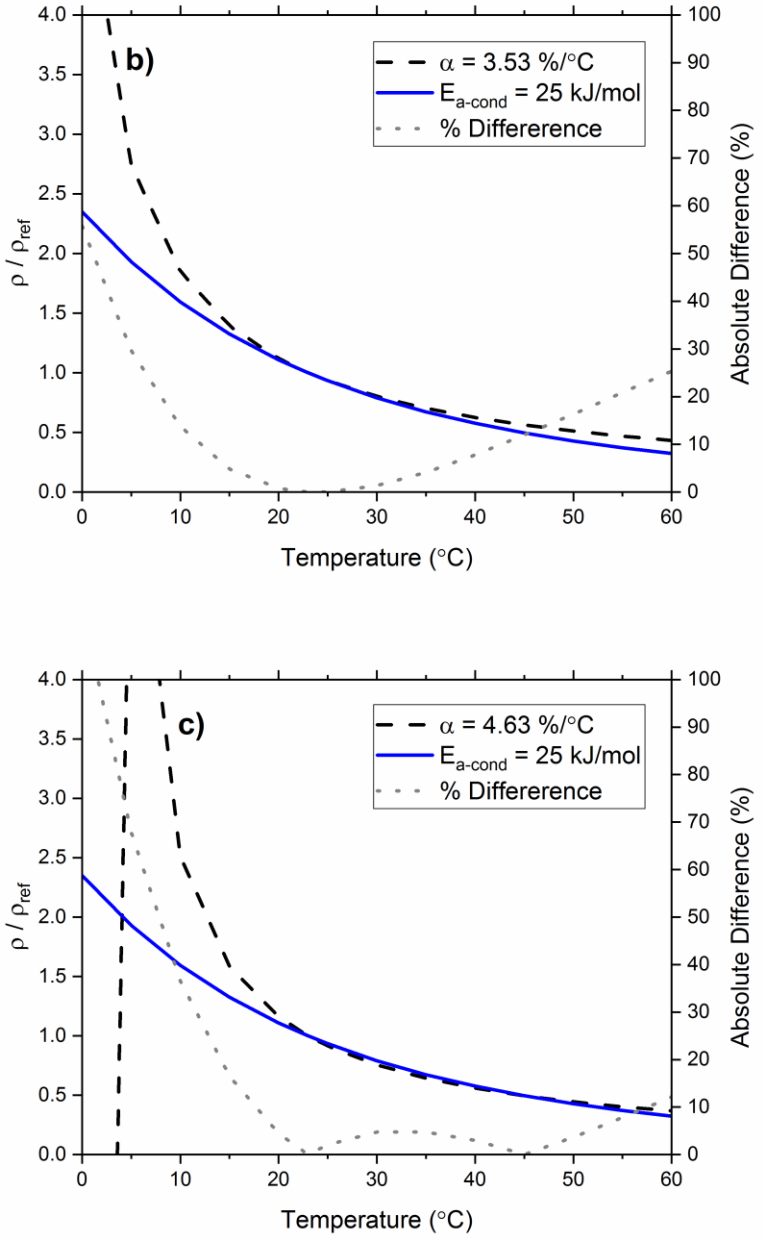

Figure 2-3 a) Temperature corrections with T_{ref} = 23°C, $E_{a\text{-}cond}$ = 25 kJ/mol showing a) α = 2.68 %/°C b) α = 3.53 %/°C, and c) α = 4.63%/°C.

2.5.2 Changing Concrete Degree of Saturation

Comparing α and $E_{a\text{-}cond}$ values to measured data enables the differences between these corrections to be observed. This is shown using resistivity measurements

on sample FA-3 (sealed cured condition and T_{ref} = 23°C). Eq. 2-2 can be rewritten to solve for α as

$$\alpha = \frac{\left(\frac{1}{\rho} - \frac{1}{\rho_{Tref}}\right)\cdot 100}{\left(T - T_{ref}\right)\frac{1}{\rho_{Tref}}} \qquad (2\text{-}5)$$

There are multiple ways to fit α to a set of measured data. One method would be to take two points and plug them into Eq. 2-2. Another method would be to obtain an average α of all points measured by taking the slope of 1/ρ vs. T and normalizing to $1/\rho_{Tref}$.

Both cases were examined using two points with three different temperatures points for reference (i.e., T_{ref} = 23°C and T = 7°C, 15°C, 33°C), and a slope of the entire range of measurements. Figure 2-4a shows a comparison of the measured data with these four fits and Figure 2-4b shows the error between the measured data and these four fits. The error is calculated as the difference between the measured and fitted value divided by the measured value. From Figure 2-4a it is apparent that at lower temperatures, the four different fits deviate from each other and errors may increase, consistent with the interpretation of the results from Figure 2-3. The results shown in Figure 2-4b indicate that the maximum error values range from -5% to 35%.

When corrections using two discrete temperature points are considered, the error at the two points is zero by definition. Between the two temperatures, the error is relatively small and negative. Outside this range the error is positive and increases. This can be seen when considering error at low temperatures when T = 33°C. This is due to corrections using α being unstable at lower temperatures, as shown in Figure 2-

3. Therefore, when using two point corrections, the second temperature should be selected within the range of interest.

When using the slope correction, the error is averaged through the entire testing temperature range, instead of being minimized at specific temperatures. The errors obtained with the slope correction lie between the errors obtained using T = 7°C and 33°C.

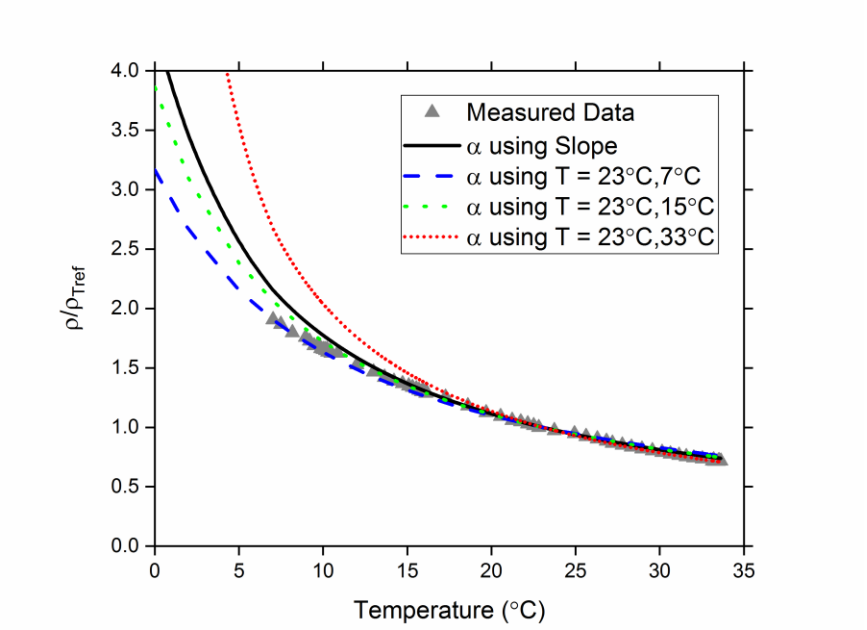

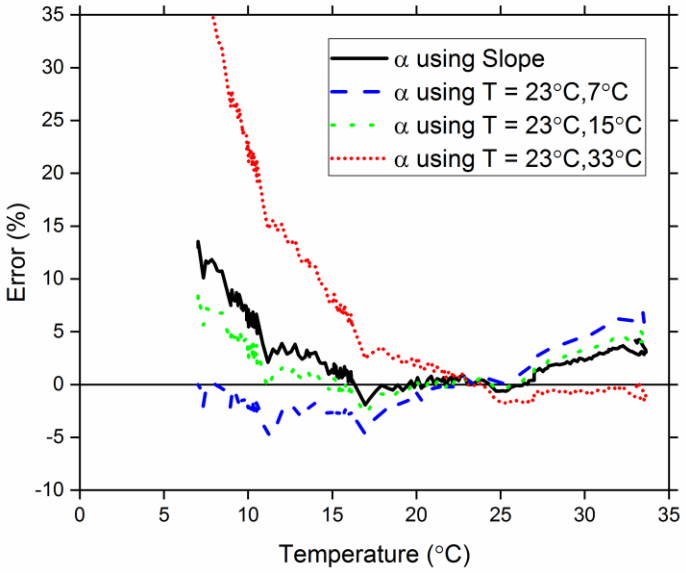

Figure 2-4 a) Temperature correction using three methods to determine α, and b) Error between measured data and fitted curves, with zero error at the reference of 23 °C.

The process is repeated by fitting the same set of measured data using an $E_{a\text{-}cond}$ approach. Eq. 2-3 can be rewritten to solve for $E_{a\text{-}cond}$.

$$E_{a-cond} = \frac{\ln(\rho) - \ln(\rho_{Tref})}{\left(\frac{1}{T} - \frac{1}{T_{ref}}\right)} \cdot \mathrm{R} \qquad (2\text{-}6)$$

The slope correction is performed by plotting ln(ρ) vs. 1/T, taking the average slope, and multiplying it by the universal gas constant R. The discrete temperature corrections were performed using three cases, taking the slope of points at T_{ref} = 23°C and a variety of second temperatures (T = 7°C, 15°C, 33°C). Figure 2-5a shows a comparison between these four approaches and Figure 2-5b shows the associated error, calculated as the difference between the measured and fitted value divided by the measured value.

Figure 2-5a shows that the different correction methods fit the data more closely than the corrections using α regardless of the method used. This is confirmed by Figure 2-5b, where the errors are lower than with α (between -7% and 2%). The errors show similar trends to those seen with errors in α though these trends are less pronounced. These results suggest that $E_{a\text{-}cond}$ is an overall better temperature correction than α. The different correction methods all result in low values of error (e.g. using a two point correction has similar error to using slope).

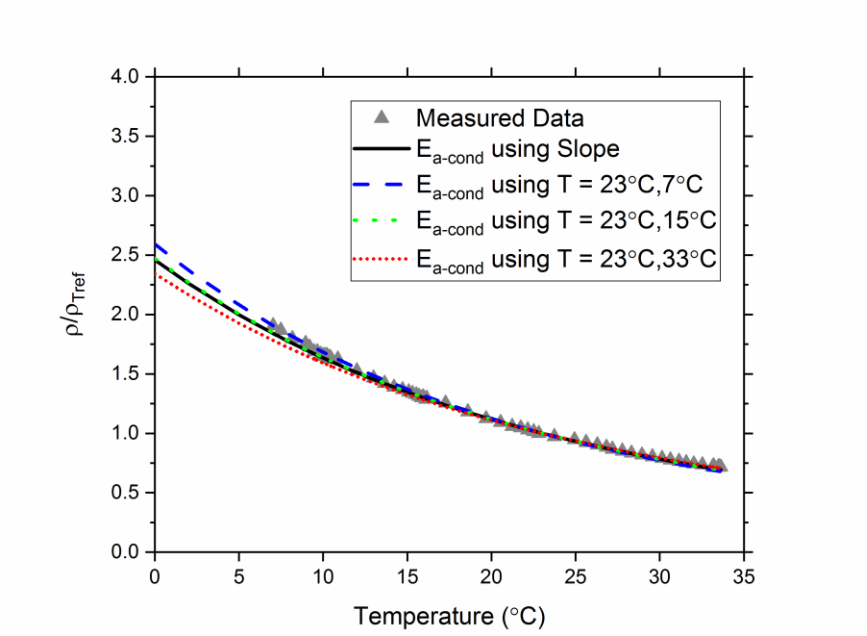

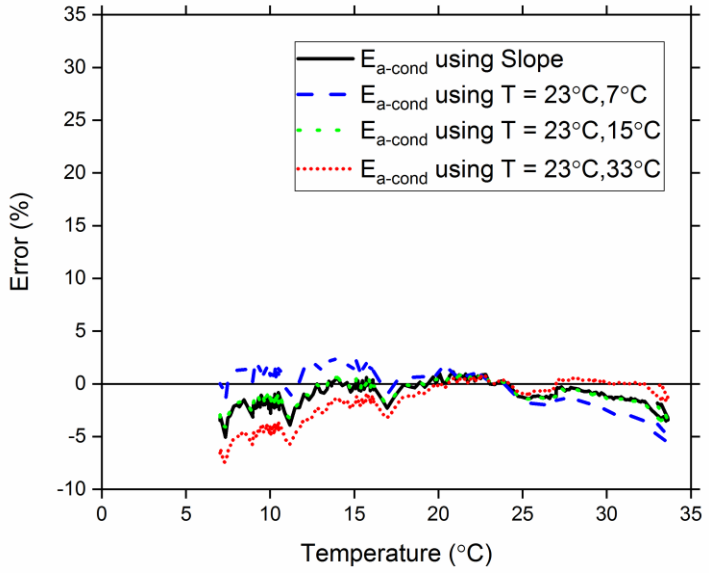

Figure 2-5 a) Temperature correction using three methods to determine $E_{a\text{-}cond}$, and b) Error between measured data and fitted curves.

2.6.3 Temperature Corrections for Saturated Samples

A comparison was made between the α and $E_{a\text{-}cond}$ fits for saturated samples (for the thirteen concretes shown in Table 2-1). For these samples the fitting was done by using the average value of the temperature corrections for the entire set of data (using T_{ref} = 25°C). Figures 2-6a and 2-6b show a comparison of the data with the fits. Percent error is plotted on the secondary axis (shown as the average error along with error bars representing ± one standard deviation).

It can be seen from these figures that for saturated specimens using average α and $E_{a\text{-}cond}$ values results in good fits for the entire data set with error below 10%. These errors slightly increase at lower temperatures and over the range of temperatures, the fit using $E_{a\text{-}cond}$ is marginally better than the fit with α.

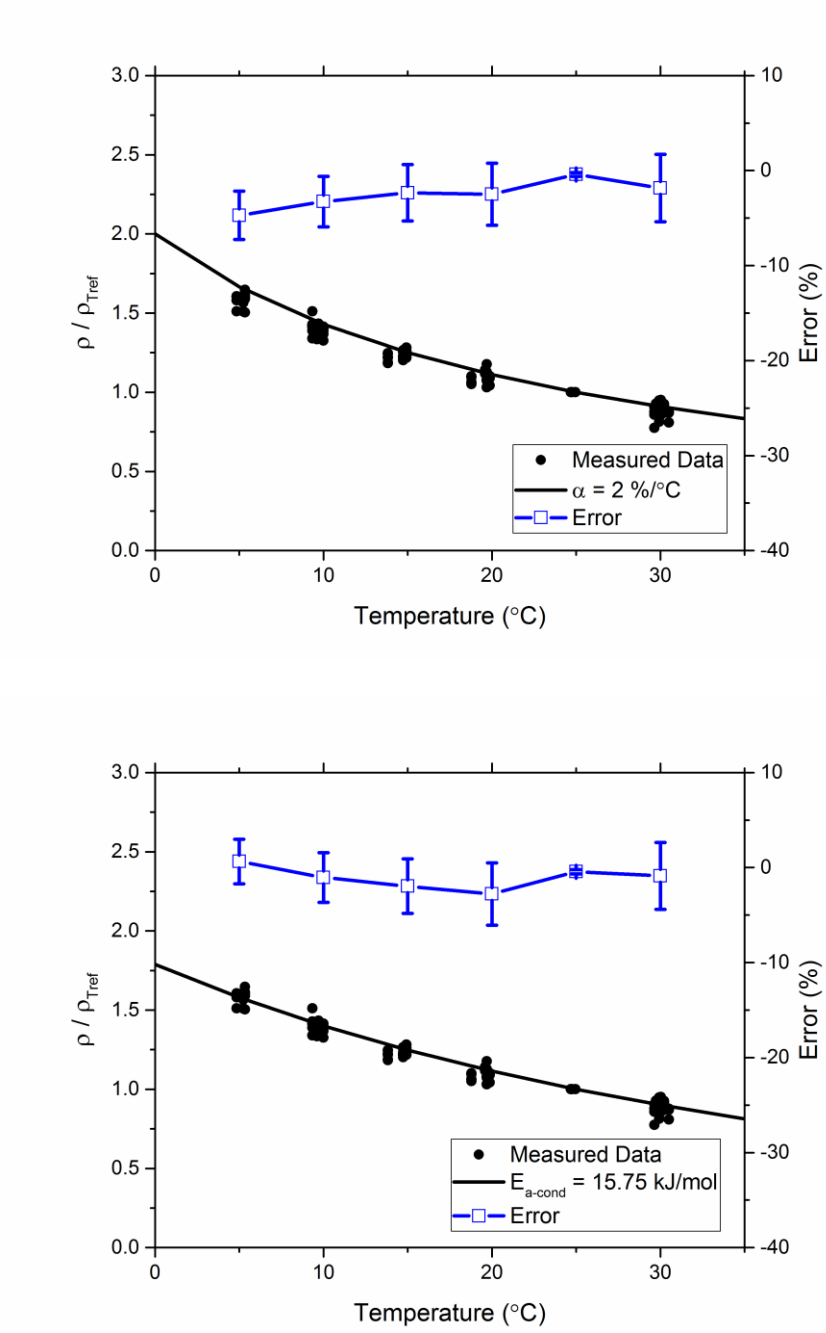

Figure 2-6 Temperature corrections of saturated specimens with an average a) α = 2.00 %/°C b) $E_{a\text{-}cond}$ = 15.75 kJ/mol. The average error between measured data and the fits is shown with ± one standard deviation.

2.6.4 Temperature Corrections for Sealed Specimens

In a manner similar to that done for saturated specimens, a comparison was made to evaluate the fits using α and $E_{a\text{-}cond}$ for a set of specimens in sealed conditions by using the average values for the entire set of data (using T_{ref} = 25°C). Figures 2-7a and 2-7b show a comparison of the data with the fits. Percent error is plotted on the secondary axis (shown as the average error along with error bars representing ± one standard deviation).

Using an α temperature correction at higher temperatures results in lower errors (average error less than 10%) however, there is increasing error in the fits at lower temperatures. The average error ranges from 5% to 20% when using the α correction. The errors when using the $E_{a\text{-}cond}$ correction are lower than when using the α correction, ranging from 0% to 5%.

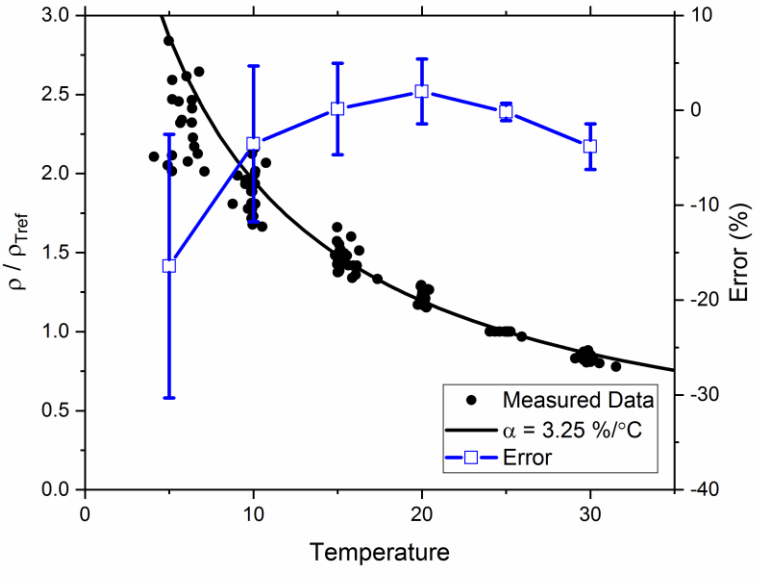

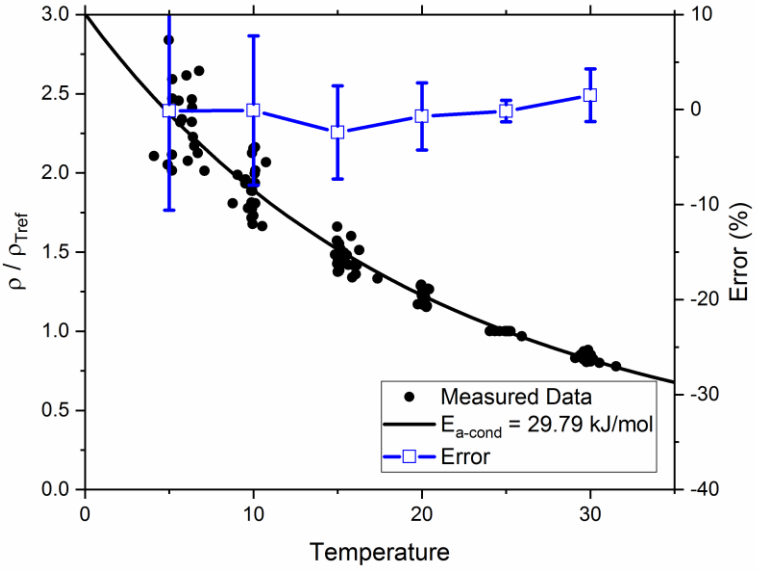

Figure 2-7 Temperature corrections of sealed specimens with an average a) α = 3.25 %/°C b) $E_{a\text{-}cond}$ = 29.79 kJ/mol. The average error between measured data and the fits is shown with ± one standard deviation.

The associated temperature correction and error values for sealed and saturated specimens are summarized in Table 2-2. The average, the standard deviation, and the coefficient of variation of the values of $E_{a\text{-}cond}$ and α for the measurements are also shown in Table 2-2.

Saturated specimens have lower values of $E_{a\text{-}cond}$ and α. For saturated specimens, both corrections $E_{a\text{-}cond}$ and α exhibited low error (2.78% for $E_{a\text{-}cond}$ and 4.72% for α). For saturated samples, $E_{a\text{-}cond}$ had a lower coefficient of variation (CoV) than α (4.39% compared to 8.21%). This suggests that in cases of low temperature sensitivity (low values of α or $E_{a\text{-}cond}$), both temperature corrections provide similar predictive capabilities with similar error values. This is a possible explanation for why α is a popular temperature correction for solutions, which typically have lower

temperature sensitivities (*51–54*). Another study has also noted that saturated concrete specimens did not show much variation in their $E_{a\text{-}cond}$ values (*25*).

The electrical measurements of sealed specimens are more temperature sensitive, and have higher values of $E_{a\text{-}cond}$ and α than saturated specimens. For sealed systems, the errors are higher (2.41% for $E_{a\text{-}cond}$ and 16.42% for α). Using α in this set of data results in larger errors at lower temperatures. This suggests that $E_{a\text{-}cond}$ is a better representation of the resistivity-temperature dependence and is a more stable and reliable correction method and the authors suggest that resistivity data should be fit with $E_{a\text{-}cond}$ (especially for sealed specimens) especially since α provides no other advantages and is just as time consuming to compute.

Table 2-2 Summary of temperature corrections for saturated and sealed samples.

	Saturated Specimens	**Sealed Specimens**
$E_{a\text{-}cond}$ (kJ/mol)	15.75	29.79
Error (%)	2.78	2.41
Standard deviation (kJ/mol)	0.69	3.22
CoV (%)	4.39	10.8
α (%/°C)	2.00	3.25
Error (%)	4.72	16.42
Standard deviation (%/°C)	0.16	0.29
CoV (%)	8.21	8.97

2.6.5 Determining $E_{a\text{-}cond}$ and α

Without any other information provided apart from the saturation state of the sample, it is suggested based on the results that using the following values of $E_{a\text{-}cond}$ and α would be reasonably acceptable: a) for saturated conditions, $E_{a\text{-}cond}$ = 15.8 kJ/mol and α =2.00 %/°C; and b) for sealed conditions, $E_{a\text{-}cond}$ = 29.8 kJ/mol and α =3.25 %/°C. For specimens with an unclear saturation state, $E_{a\text{-}cond}$ values from

literature have been reported to be 15 – 22 kJ/mol in one study and 16 – 30 kJ/mol in another study. Both of these ranges are consistent with the results reported here (*8*, *55*).

2.7 Conclusions

This study assesses the influence of temperature on the electrical resistivity of concrete and discusses a procedure to correct for temperature. A linear temperature correction approach (α) and an activation energy correction ($E_{a\text{-}cond}$) approach were evaluated. These approaches were compared to each other and with measured data. The results indicate that for systems where resistivity has a low temperature sensitivity, $E_{a\text{-}cond}$ (0-15 kJ/mol), predictions using the two approaches were mathematically comparable and related to each other nearly linearly. However, for systems with a higher $E_{a\text{-}cond}$ (15-45 kJ/mol), the relationship between $E_{a\text{-}cond}$ and □ are non linear and predictions using an $E_{a\text{-}cond}$ approach were more accurate over a wide temperature range. These corrections were studied for sealed and saturated concretes with a variety of mixture designs. Average values for $E_{a\text{-}cond}$ were found to be 29.8 kJ/mol for sealed samples and 15.8 kJ/mol for vacuum saturated samples. As such, the linear temperature correction α may be acceptable for saturated concrete specimens or extracted pore solutions. However the Arrhenius temperature correction $E_{a\text{-}cond}$ is more accurate for a wide range of conditions and particularly for higher performance concrete and concrete tested in a sealed condition. $E_{a\text{-}cond}$ is more representative of the actual resistivity-temperature relationship. Based on this study it is recommended that $E_{a\text{-}cond}$ should be used instead of α since the use of α is less

accurate over the range of temperatures and it provides no particular advantage, is measured using the same process (cycling the temperature of a concrete specimen while measuring its resistivity), and is just as time consuming to compute.

2.8 Acknowledgements

This work was conducted through the National Concrete Consortium and the mixtures were produced by members of the Performance Engineered Mixtures (PEM) Champion States. Gratitude is extended for their effort as the data shown here would not have been possible without their assistance. The experiments were conducted at the Kiewit Materials Performance Lab and Concrete Performance Lab at Oregon State University. The authors are grateful for contributions that have made the operation of the laboratory possible.

3. Factors Affecting Activation Energy of Conduction of Cementitious Materials

3.1 Abstract

This paper examines factors that influence the accuracy of temperature corrections for electrical conductivity/resistivity measurements of concrete. The Arrhenius equation is used to describe the behavior of resistivity as a function of temperature using an activation energy of conduction ($E_{a\text{-}cond}$). This parameter has been measured on a wide variety of materials and specimen geometries in the literature including pore solutions, pastes, mortars, and concretes (with a variety of saturation states) with reported values typically ranging from 9 to 39 kJ/mol. In order to select an appropriate $E_{a\text{-}cond}$, it is important to understand the factors affecting $E_{a\text{-}cond}$ of cementitious materials. In this study, the $E_{a\text{-}cond}$ was determined from data measured on various concrete mixtures used in transportation infrastructure applications as well as extracted and simulated pore solutions. It was found that $E_{a\text{-}cond}$ increases as the degree of saturation of the specimen is reduced with an average$E_{a\text{-}cond}$ value of 15.8 kJ/mol when the specimen is saturated. The $E_{a\text{-}cond}$ was measured on pore solutions with a wide range of ionic strengths. It was found that $E_{a\text{-}cond}$ of pore solutions remains relatively constant (an average value of 13.9 kJ/mol ± 1.5 kJ/mol) in the typical ranges of pore solution ionic strength and was similar to, albeit slightly lower than $E_{a\text{-}cond}$ of saturated samples. Drying increases the ionic concentration of the fluid in the pores and decreases the connectivity of the fluid filled pores. The changes in $E_{a\text{-}cond}$ due to drying were determined to be primarily due to a change in the connectivity of the fluid filled pores as opposed to concentrating the pore solution. Under certain circumstances, changes in ionic mobility due to changes in viscosity,

may also affect the measured $E_{a\text{-}cond}$. While it is better to directly measure the $E_{a\text{-}cond}$ of every single concrete mixture, this is not always feasible or practical. In such cases, for pore solutions a value of 13.9 kJ/mol can be used and for saturated concretes a value of 15.8 kJ/mol can be used. For concretes with a varying degree of saturation, the $E_{a\text{-}cond}$ can be estimated if the degree of saturation (DOS) is known using the equation:

$$E_{a-cond} = 33.3 - 16.3 \cdot DOS$$

3.2 Introduction

The formation factor is a material property that is equal to the inverse of the connectivity and volume of the pore network in a porous media (*27*). For concrete, the formation factor describes the transport of ions through the concrete and can be related to an effective diffusion coefficient (*32*, *33*, *39*). For a given material, the formation factor is given in Eq. 3-1:

$$F = \frac{1}{\phi\beta} = \frac{\rho}{\rho_0} \tag{3-1}$$

where F is formation factor (unitless), ϕ is the fluid filled porosity (unitless), β is the connectivity of the pores(unitless), ρ is the total bulk resistivity (Ωm), and ρ_0 is the resistivity of the pore solution (Ωm).

The formation factor of concrete materials is typically determined from electrical resistivity measurements of the bulk specimen and its corresponding pore solution. Resistivity measurements are popular and widely used primarily for their ease of use and ability to perform rapid, instantaneous measurements (*5*, *6*, *32*, *37*).

However, these measurements are dependent on several factors such as temperature (*8*, *14*, *34*, *35*), specimen geometry (*18*), conditioning (*3*, *20*, *22*, *32*, *33*), and the pore solution composition (*32*, *43*, *44*).

It is vital to correct resistivity measurements for temperature especially when examining specimens from the field, where conditions may not be controlled (*56*). The effect of temperature on resistivity measurements on cementitious materials has been detailed in prior work and different corrections have been proposed (*23*, *24*, *35*) including a linear correction and an activation energy of conduction (Arrhenius) type of approach. A method of converting the linear correction to an activation energy of conduction ($E_{a\text{-}cond}$) has been outlined in the literature (*56*).

An $E_{a\text{-}cond}$ correction has been chosen for this study as it has been shown to have advantages over a linear correction (*56*). The specimen resistivity can be corrected to a resistivity at a reference temperature using Eq. 3-2.

$$\rho_{Tref} = \rho_T \exp\left[\frac{-E_{a-cond}}{R}\left(\frac{1}{T+273}-\frac{1}{Tref+273}\right)\right] \quad (3\text{-}2)$$

where ρ_T and ρ_{Tref} are the resistivities of concrete (Ωm), T and $Tref$ (typically 23°C in the U.S.) are the temperatures of the concretes (°C), $E_{a\text{-}cond}$ is the activation energy of conduction, kJ/mol, and R is the universal gas constant, 8.314 J/(mol K).

Higher values of $E_{a\text{-}cond}$ correspond to a higher sensitivity to temperature with respect to resistivity measurements. Previous studies on temperature corrections in cementitious materials have produced a wide range of fitting parameters (*8*, *23–25*, *34–36*). These results are summarized in Table 1 and show the reported values of $E_{a\text{-}cond}$, specimen type (i.e., concrete, mortar, paste), storage condition and degree of

saturation (DOS), and water-to-cementitious material ratio (w/cm).

Table 3-1 Reported values of $E_{a\text{-}cond}$ from various studies.

Source	$E_{a\text{-}cond}$ (kJ/mol)	Type	Condition	w/cm
Whittington et al. (1981) (*23*)	17.7[a]	Paste	Saturated	0.40-0.80
Elkey and Sellevold (1995) (*25*)	14.0[a]	Concrete	Saturated	0.40,0.60
	39.0[a]		25% DOS	
McCarter et al. (1995) (*24*)	19.4	Mortar	Saturated	0.40
Chrisp et al. (2001) (*34*)	25.7	Concrete	Saturated	0.40-0.44
	39.1	Concrete	50% RH	0.40-0.44
Julio Bentancourt et al. (2004) (*8*)	19.7[a]	Concrete	Saturated (RCPT)	0.25-0.79
Sant et al. (2008) (*35*)	25.6-27.6	Paste	Sealed	0.30
	8.9-13.5	Pore Solution	Simulated	-
Castro et al. (2010) (*36*)	9.7-10.2	Pore Solution	Extracted from sealed paste	0.36-0.50

[a] indicates reported originally in units of K from Hinrichson-Rash law

According to these results, values of $E_{a\text{-}cond}$ for pore solutions range between 8.9 to 13.5 kJ/mol. For concretes, the corresponding range is 14.0 to 39.1 kJ/mol, depending on the moisture state of the specimen. Choosing an incorrect $E_{a\text{-}cond}$ can lead to errors in the temperature correction curves, therefore, it is important to select an $E_{a\text{-}cond}$ appropriate for a given scenario.

3.3 Research Objectives

While studies in literature have explored temperature corrections in electrical measurements for concrete, numerous values of temperature correction coefficients have been reported. While it is better to measure temperature correction coefficients on a certain specimen subject to specific conditions, this is not always feasible,

especially when using temperature corrections in modeling. Therefore the objectives of this paper are to:

- Describe why there is a large variation reported in literature for $E_{a\text{-}cond}$ values
- Outline the physical mechanisms behind the differences in $E_{a\text{-}cond}$ values
- Provide guidance on choosing correct $E_{a\text{-}cond}$ values

3.4 Materials

As part of a multi-laboratory study, cylindrical concrete specimens (100 mm diameter by 200 mm length) representing different pavement or bridge deck mixture designs were cast and shipped from several locations across the United States. The mixture designs are summarized in Table 3-2.

Specimens were sealed during curing to avoid alkali leaching (*20*), because it is a more consistent curing condition than either moist curing or fogging, and for ease of storage and transportation. The specimens were cast and remained in their original plastic molds, and were additionally double bagged with plastic bags after being cast. The specimens were kept sealed at room temperature after being received until an age of 180 days, at which time the specimens were subjected to the testing program.

Table 3-2 Mixture proportions of the concretes used in this study with Na_2O equivalent available alkali contents from mill certificates indicated in square brackets.

Mixture ID	**w/cm**	**Water (kg/m^3)**	**Cement (kg/m^3)**	**Fly Ash (kg/m^3)**	**Slag (kg/m^3)**	**Air (%)**	**Aggregate (kg/m^3)**
M1	0.41	161	390 [1.09]	-	-	6.5	1738
M2	0.40	135	335[b] [0.64]	-	-	7.3	1790
M3	0.39	122	248 [0.6]	62 [2.78][d]	-	6.8	1906
M4	0.37	154	332 [0.52]	82 [0.92]	-	5.0	1749
M5	0.44	143	279 [0.73]	43 [1.11]	-	7.0	1817
M6	0.42	142	273 [0.52]	68 [1.38]	-	6.5	1837
M7	0.43	141	247[c] [0.58]	-	82	6.0	1820
M8	0.40	131	262 [0.54]	66 [1.30]	-	6.0	1805
M9	0.43	136	205 [0.55]	47 [1.90]	65	5.5-8.0	1878

[b] denotes an ASTM C595 IP(25) cement (*45*)
[c] denotes an ASTM C595 IS(20) cement (*45*)
[d] denotes total alkali content

3.5 Experimental Techniques

3.5.1 Concrete Testing Apparatus: Resistivity and Temperature Cycle

After preparing the top and bottom surfaces of the concrete cylinders for proper adhesion with a #20 grit concrete sanding block, a conductive nickel coating was applied to the top and bottom surfaces. The nickel coating serves as a permanent electrode to be used in uniaxial bulk resistivity measurements (*46*, *47*) eliminating the need for a saturated sponge and the associated effects of the sponge drying over time. The impedance and phase angle of the specimens were measured using a Giatec RCON2™ resistivity meter.

The outer circumferences of the cylindrical specimens were covered in plastic to prevent moisture loss while tests were being performed. Additionally, aluminum tape was applied to the top and bottom of the sample to prevent moisture loss as well as to ensure a connection between the leads of the resistivity meter and the electrodes.

An apparatus consisting of copper cooling coils connected to a water bath was constructed allowing for six 100 by 200 mm concrete cylinders to be tested simultaneously. The copper coils surround the specimen controlling temperature from the outside. Additional details of the setup are described in a prior study (*56*). A well-hydrated spare concrete cylinder was cast with an embedded thermistor with an accuracy of 0.1 °C and is used as a representative quantifier of the temperature of all the specimens. The concrete specimens were placed in the remaining coils. The temperature of the water bath was first lowered and kept at 5°C until the specimen temperature equilibrated. Resistivity measurements were taken between temperature steps, at the time of equilibrium. The temperature was increased at specified set-points from 5°C to 30°C in 5°C increments. This range represented a range of temperature typically found in the field and ensured there were no effects from freezing (*46, 57*).

3.5.2 Degree of Saturation (DOS)

The DOS of a specimen is defined as the ratio of liquid in a specimen to the total volume of liquid the specimen can hold, or the percentage of voids that are filled in a porous specimen. At the testing age of 180 days, samples were first dried in a 110°C ± 5°C oven until their mass equilibrated and was recorded as m_{od}. The

specimens were placed in a chamber under a vacuum at an absolute pressure of 10 ± 3 torr for three hours. While still under vacuum, deaerated saturated calcium hydroxide solution was added and samples were soaked for one additional hour before removing from the vacuum chamber. Samples remained under water for an additional 24 hours before testing. Samples were removed from the solution and their masses measured, defined as m_{sat} at DOS=100 %. The vacuum saturation process is outlined in prior work (*49*).

After measuring $E_{a\text{-}cond}$ (using the cooling coils and the resistivity meter) at the saturated state, the samples were left to dry in open air until a desired mass was lost. The specimens were sealed and double bagged for a period of one week to allow the moisture to equilibrate. The specimens were then debagged, their masses were recorded as m_i, and they were placed into the cooling coil apparatus to measure $E_{a\text{-}cond}$. This process was repeated for multiple DOS values. The DOS for each specimen was calculated as shown in Eq. 3-3.

$$DOS = \frac{\left(m_i - m_{od}\right)}{\left(m_{sat} - m_{od}\right)} \tag{3-3}$$

where m_i is the mass of the specimen measured immediately before being placed in the cooling coil (g), m_{od} is the oven dried mass (g), and m_{sat} is the mass of the specimen after it has been vacuum saturated (g).

3.5.3 Pore Solution Extraction and Measurement

Paste specimens were cast with raw materials from each of the mixtures in Table 3-2 using the paste portions of the mixture designs. Pastes were prepared in a vacuum mixer and cast into 35.8 by 55.4 mm canisters and sealed cured. Specimens

were placed on a rotating jar mill for the first 24 hours to prevent bleeding, and then subsequently cured under ambient conditions (23 °C). Pore solutions were extracted at 7 and 14 days to quantify the impact of the ionic composition on $E_{a\text{-}cond}$. Pore solution compositions at 14 days showed only slight variation from 7 day compositions and are therefore not discussed. Approximately 250 g of paste was crushed using a mortar and pestle to obtain fragments no larger than 10 mm. Pore solution was extracted using a high pressure steel die as described in prior literature (*31*). The pieces were loaded to 2220 kN with the load rate between 444 kN/min to 890 kN/min.

The resistivity of the extracted pore solution was measured using a conductivity cell constructed of a polycarbonate tube with a diameter of 9.53 mm and a length of 25.4 mm fitted to two electrodes made of brass similar to that described in literature (*36, 58*). The pore solution resistivity cell is connected to a Giatec RCON2™ resistivity meter where its impedance is measured at a selected 7 kHz frequency in order to ensure a low phase angle (*57*).

Activation energy was measured by first filling the pore solution cell with pore fluid and placing it in a 5°C chamber where the temperature was allowed to equilibrate. Once the temperature reached equilibrium, the cell was taken out and a thermistor was placed into the filling port of the cell to measure the temperature of the fluid. Temperature and impedance were measured as the temperature of the pore solution was allowed to equilibrate up to room temperature.

Additionally, the extracted pore solutions were fused into beads using a fusion device and then the ionic compositions of these solutions were measured using a

calibrated X-ray fluorescence (XRF) device in a method outlined in literature (*59*). Since the age of the pore solution is after one day and the sulfate is depleted, it is assumed that the significant ions in solution are sodium, potassium, and hydroxide ions (*19*). Sodium and potassium were measured using the XRF and the concentrations of hydroxide ions was calculated based on it balancing the ionic strength of potassium and sodium. The ionic strength and resistivities of the pore solutions were calculated using a method outlined elsewhere (*30*). The calculated resistivities from the XRF agree well with measured resistivities and are not discussed in detail here.

3.6 Results and Discussion

3.6.1 Role of Degree of Saturation

From Table 3-1, it is apparent that there is a large variation reported in literature for $E_{a\text{-}cond}$ values. This variation can be attributed to two reasons. First, the moisture condition, or DOS, affects $E_{a\text{-}cond}$ (*25*, *34*). Second, reported $E_{a\text{-}cond}$ values of pore solutions have lower values than that of pastes, mortars or concretes.

The effect of DOS on $E_{a\text{-}cond}$ is shown for the mixtures M6, M7, and M8 in Fig. 1. The different DOS values were obtained by vacuum saturating specimens to achieve a maximum DOS and subsequent drying to achieve different DOS values followed by sealing to allow for moisture to equilibrate, as outlined in earlier sections. $E_{a\text{-}cond}$ was measured at each DOS value. Additionally, the measured $E_{a\text{-}cond}$ of the corresponding pore solution is plotted as a dotted line for these samples (as pore solutions do not have a DOS).

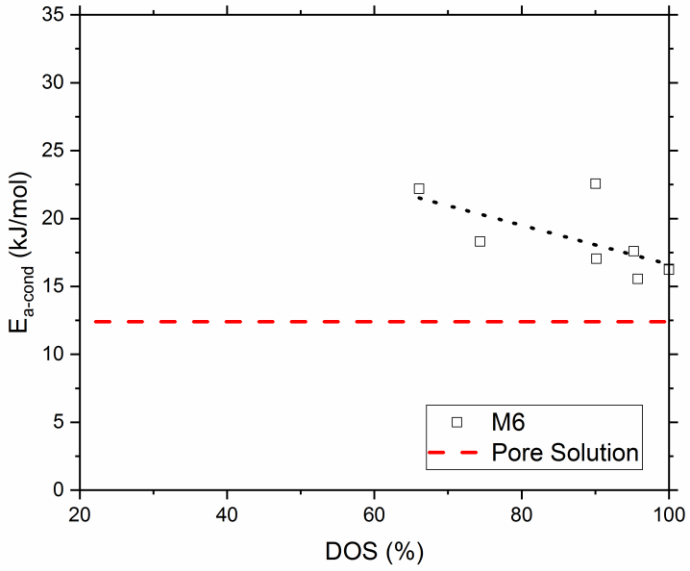
35
30
25
20
15
10
5
0
20
40
60
80
100
$E_{a\text{-}cond}$ (kJ/mol)
DOS (%)
M6
Pore Solution

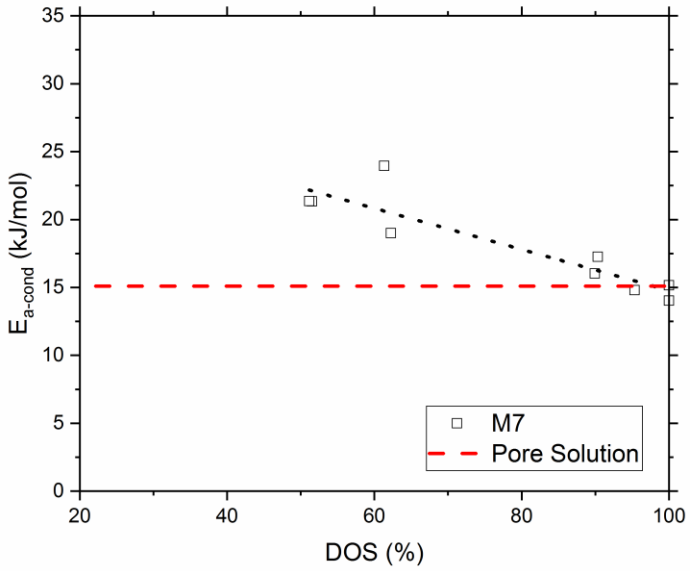
35
30
25
20
15
10
5
0
20
40
60
80
100
$E_{a\text{-}cond}$ (kJ/mol)
DOS (%)
M7
Pore Solution

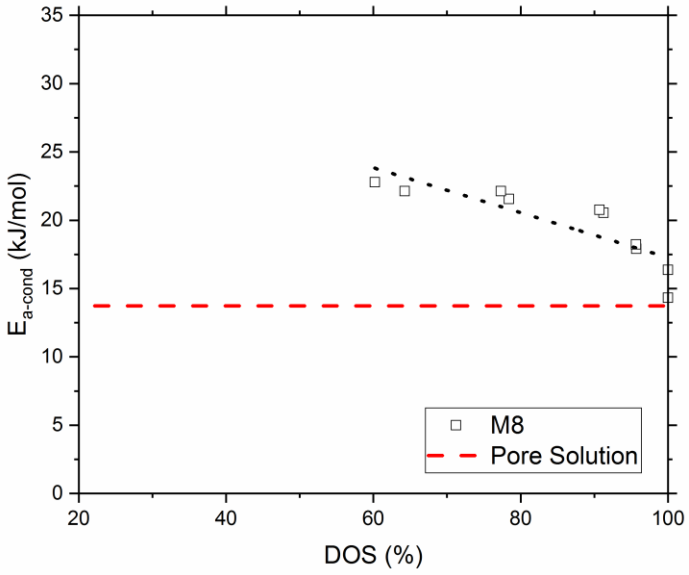

Figure 3-1 $E_{a\text{-}cond}$ for various DOS where the red dashed line represents the $E_{a\text{-}cond}$ of the expressed pore solution and the black dotted line is a linear fit to illustrate at higher degrees of saturation, $E_{a\text{-}cond}$ of concrete approaches the value of the pore solution, for Mixtures (a) M6, (b) M7, (c) M8.

Fig. 1 shows that a decrease in the DOS of the concrete results in an increase in $E_{a\text{-}cond}$. There is an approximate linear trend, however, the slopes of these lines are different for each of these mixtures and scatter in the data exists. The slopes, intercepts at 0 and 100% DOS, and R^2 values are summarized in Table 3-3.

Table 3-3 Summary of $E_{a\text{-}cond}$ fitted to DOS.

Mixture ID	**Slope**	**$E_{a\text{-}cond}$ at 0% DOS**	**$E_{a\text{-}cond}$ at 100% DOS**	**R^2**
M1	13.4	32.0	18.7	0.39
M2	29.8	46.2	16.4	0.89
M3	19.0	35.4	16.4	0.78
M4	32.6	48.9	16.3	0.77
M5	15.7	32.6	16.9	0.91
M6	14.4	31.0	16.6	0.43
M7	15.1	29.9	14.8	0.83
M8	16.4	33.7	17.3	0.71
M9	21.7	37.6	16.0	0.88

The slopes of the lines for all the mixtures range from -13.4 to -32.6. The correlations of these fits vary with ranges between 0.4 and 0.9. It should be noted that M1 and M6 have a weaker linear relationship with an R^2 less than 0.5. This may be due to the small sample size where one outlier will throw off the R^2 value as seen in Fig. 3-1a.

The measured $E_{a\text{-}cond}$ value of the pore solution was generally equal to or lower than that of the saturated specimens. As the pore solution is extracted from sealed paste samples, its ionic composition may be different from the ionic concentration of the pore solution in the saturated concrete. In addition, the concrete has a tortuous pore network which may change the $E_{a\text{-}cond}$. These factors can help to explain differences between the $E_{a\text{-}cond}$ values of the extracted pore solution and the saturated concrete, but the general trend is observed that as the concrete becomes closer to full saturation, the temperature sensitivity with respect to electrical measurements approaches the behavior seen in extracted pore solutions.

The same process is repeated for all the specimens in the set of mixtures. The measured $E_{a\text{-}cond}$ values of all specimens are plotted together in a single plot at their respective DOS in Fig. 3-2.

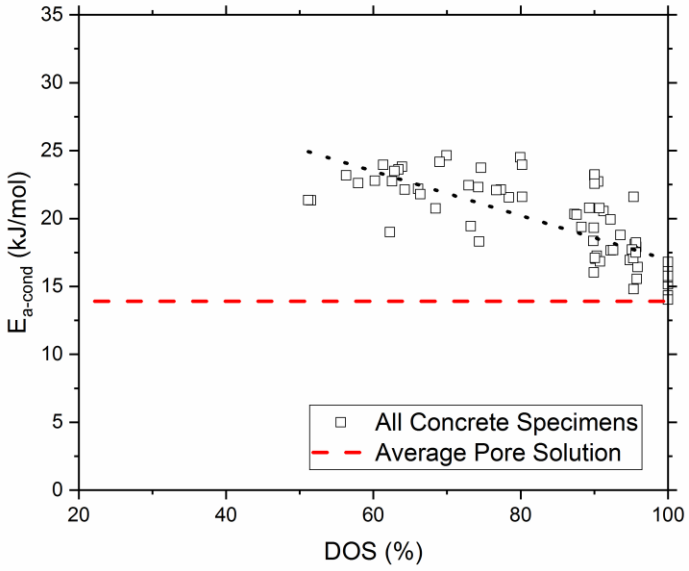

Figure 3-2 $E_{a\text{-}cond}$ of all mixes plotted for various DOS.

Fig. 3-2 shows a similar trend to Fig. 3-1, where, as DOS increases, $E_{a\text{-}cond}$ decreases. However, this trend is not as strong as the individual relationships for each mixture (with an average R^2 of 0.7) and has a lower R^2 value of 0.6. The average $E_{a\text{-}cond}$ value of the pore solutions was 13.9 kJ/mol which is lower than that of the average $E_{a\text{-}cond}$ values of saturated specimens, 15.8 kJ/mol. The equation of the line is shown in Eq 3-4.

$$E_{a-cond} = 33.3 - 16.3 \cdot DOS \quad (3\text{-}4)$$

Eq. 3-4 and Fig. 2 are a good starting point in determining a unique $E_{a\text{-}cond}$ for a specimen if the DOS is known. A similar relationship between $E_{a\text{-}cond}$ and DOS has been shown in literature with values of around 24 kJ/mol at 57% DOS and 14 kJ/mol at full saturation (*25*).

Simply stating that $E_{a\text{-}cond}$ is a function of DOS is useful from a practical perspective. It is however of scientific interest to understand the underlying

mechanisms behind this relationship, as DOS has complex effects on the specimen resistivity. Eq 3-1 shows that bulk resistivity is a function of the pore solution resistivity (ρ_0) and the porosity and connectivity of the pores (ϕ β). As the pores empty, the ions remain in the pores and the pore solution becomes more concentrated. This effectively decreases the pore solution resistivity (ρ_0) and could potentially affect $E_{a\text{-}cond}$. As the pores empty, the fluid filled porosity (ϕ) is reduced, the connections between the fluid filled pores are modified and the connectivity of the pores (β) decreases. Therefore, the effects of DOS on $E_{a\text{-}cond}$ must be due to a change in the pore solution resistivity or due to a change in the connectivity of the pores.

3.6.2 Role of Ionic Strength of Pore Solution

The effect of increasing ionic strength on $E_{a\text{-}cond}$ was studied by measuring the resistivity of various ionic solutions using a solution cell while varying the temperature. Pore solutions were extracted from sealed paste samples of the same material as the concretes. The ionic compositions were measured with XRF (*59*) to determine their ionic strength as explained earlier (*30*). For these solutions, the $E_{a\text{-}cond}$ is plotted as a function of their ionic strength in Fig. 3-3. In addition, solutions of 0.25, 0.5, 1, and 2 mol/L NaOH (representative of a simulated pore solution undergoing drying) were prepared, measured, and their $E_{a\text{-}cond}$ values are also shown in Fig. 3-3.

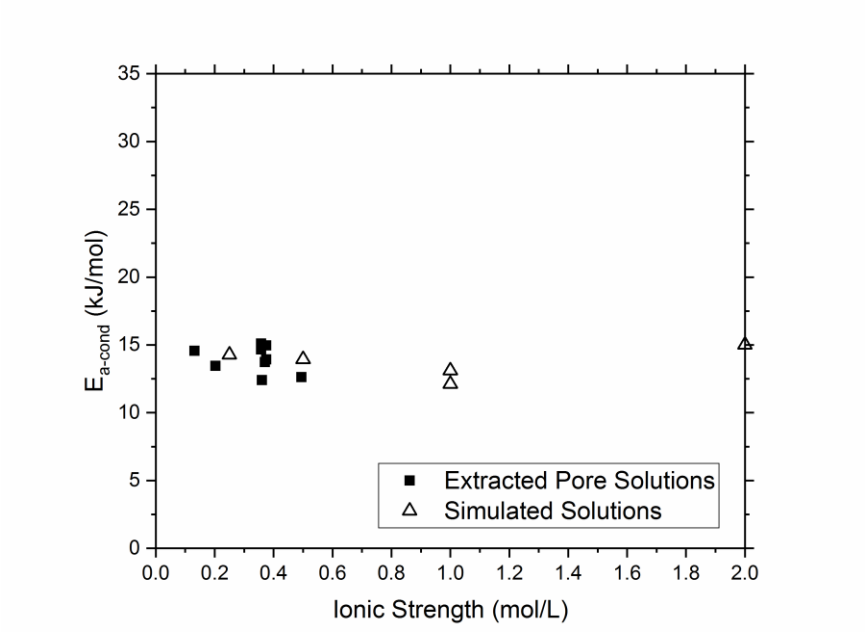

Figure 3-3 Effect of solution ionic strength on $E_{a\text{-}cond}$ using extracted pore solutions and simulated solutions consisting of NaOH.

The measured data shows that there is no appreciable change in $E_{a\text{-}cond}$ with respect to ionic concentration in the range of 0.25 to 2 mol/L. This holds true for extracted pore solutions and for simulated pore solutions. At approximately the same ionic strength, there is a slight scatter in the $E_{a\text{-}cond}$ values, which could be attributed to potential interactions between multiple ionic species that are present in the pore solution, including potassium, sodium, calcium, hydroxide, and sulfate ions. The artificial solutions were made using only sodium hydroxide, and show less scatter. These results contradict a study in literature showing that an increase in pore solution ionic strength results in a decrease in $E_{a\text{-}cond}$ ranging between 9 kJ/mol and 14 kJ/mol (*35*), however, as several solutions and simulated solutions of a range of ionic strength have been tested, the obtained conclusion seems reasonable. These results suggest that a change in the pore solution ionic strength is not the main reason why $E_{a\text{-}cond}$ changes with DOS and there is another dominating factor.

3.6.3 Role of Connectivity of the Fluid Filled Pores

An alternate reason why DOS affects $E_{a\text{-}cond}$ would be due to a change in the fluid filled porosity (ϕ) or connectivity of the pores (β). As DOS decreases, pores start to empty and this results in a more tortuous path that ions travel through. It is possible that ionic conduction with a longer path length will show a higher temperature dependence than ionic conduction through a shorter path length as there is more area affected by the pore wall.

The connectivity of the fluid filled pores (β') can be derived from Eq. 3-1 for a concrete specimen and is shown in Eq. 3-5 (*60*):

$$\beta' = \frac{\rho_{0-sat} \cdot DOS}{\phi_{sat} \cdot DOS \cdot \rho} = \frac{\rho_{0-sat}}{\phi_{sat} \cdot \rho} \quad (3\text{-}5)$$

where β' is the connectivity of the fluid filled pores (unitless), ϕ_{sat} is the total fluid filled porosity at saturation (unitless), $\rho_{0\text{-}sat}$ is the resistivity of the pore solution at saturation (Ωm), and ρ is the total bulk resistivity (Ωm).

On drying, both the fluid filled porosity and the pore solution resistivity decrease linearly (the latter due to an increase in the pore solution ionic concentration (*43*)) as a function of DOS. Therefore, on drying, the parameter $\rho_{0\text{-}sat}/\phi_{sat}$ remains constant for different DOS conditions.

The effect of the connectivity of the fluid filled pores can be observed by plotting $E_{a\text{-}cond}$ against β' as seen in Fig. 3-4. A log relationship between $E_{a\text{-}cond}$ and β' is apparent in the concrete specimens when plotting on a log scale. As samples increase in β', the $E_{a\text{-}cond}$ decreases. Pore solutions have a β' value of one by definition. The $E_{a\text{-}cond}$ of the pore solution represents a theoretical minimum value as

concretes with a β' of over one cannot exit. The correlation slightly improves and a higher R^2 value (0.7) is obtained when plotting $E_{a\text{-}cond}$ against β' as opposed to DOS suggesting this is a stronger relationship.

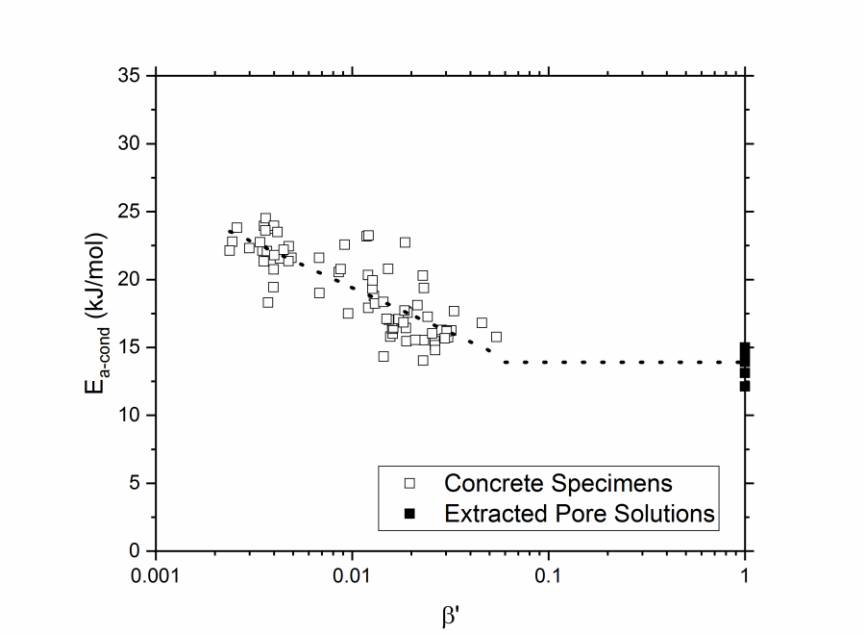

Figure 3-4 $E_{a\text{-}cond}$ of all mixtures plotted as a function of β' on a log scale.

The correlation between $E_{a\text{-}cond}$ and β' suggests that a change in the connectivity of the fluid filled pores dominates the effect of concentration of the pore solution and explains the increase in $E_{a\text{-}cond}$ as DOS decreases. This may be due to restricted ionic mobility confined to a small layer of fluid on the surface (*43*) of the pore as drying occurs and can be considered a constricting effect.

An analogy may be drawn to cases when freezing occurs in a specimen (*46*, *57*). As ice forms, a liquid–solid meniscus forms between the ice and the pore wall. Two distinct $E_{a\text{-}cond}$ values occur before and after freezing due to a constricting effect as ice forms rapidly in the bulk of the capillary pores (*46*, *57*). The $E_{a\text{-}cond}$ after freezing may represent the maximum $E_{a\text{-}cond}$ value that may be achieved.

3.6.4 Role of Ionic Mobility

The movement of ions in solution subject to an electric field is known as migration. The velocity of an ion under an electrical field, and therefore the ionic mobility, is related to the electrical force and an opposing frictional force that it experiences in the medium. This frictional force is defined in Eq. 3-6 as:

$$F_{drag} = (6\pi\eta a)s \qquad (3\text{-}6)$$

where η is viscosity (Pa·s), a is the Stokes radius of the ion (m), and s is the drift velocity of the ion(m/s).

F_{drag} may be affected by connectivity of the fluid phase as there may be some drag due to edge effects of the pore walls. This could effectively change the F_{drag} in a similar manner to that when viscosity is changed. While edge effects of pore walls are quite hard to study in practice, it is much easier to study the effect of viscosity on the $E_{a\text{-}cond}$. The viscosities of solutions have been shown to have an Arrhenius relationship with respect to temperature and therefore can be described using an activation energy of viscosity ($E_{a\text{-}visc}$) (*61, 62*).

The effect of this viscosity on $E_{a\text{-}cond}$ was studied by measuring resistivities of conductive solutions with different viscosities. Solutions of 1 mol/L NaOH were made by diluting a 2 mol/L NaOH solution with varied amounts of DI water and glycerol. The viscosities (and thus $E_{a\text{-}visc}$) of the different glycerol water mixtures are calculated at specific temperatures using an online calculator (*63*) based on equations found in literature (*64*). The ionic solution was assumed to have the same viscosity as pure water in this case. The temperature dependence of the viscosity was calculated

using different values of viscosity as determined by the calculator and applying Eq. 3-2. A plot of $E_{a\text{-}cond}$ vs $E_{a\text{-}visc}$ is shown in Fig. 3-5 and it shows a linear relationship between $E_{a\text{-}cond}$ and $E_{a\text{-}visc}$.

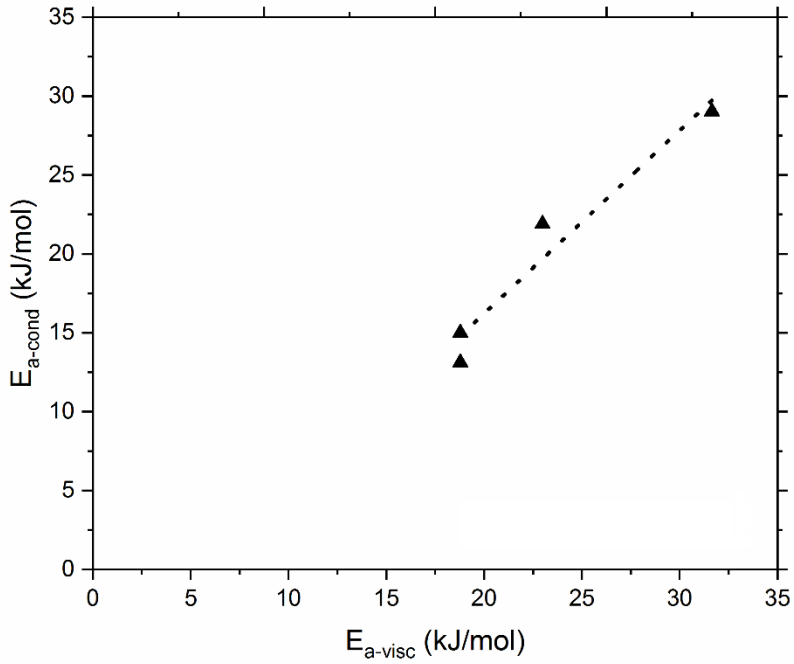

Figure 3-5 Effect of viscosity on $E_{a\text{-}cond}$.

While these results show that a change in the viscosity affects the $E_{a\text{-}cond}$, the viscosity of NaOH solutions have been shown to vary little with concentration (*65*), therefore, it is unlikely that viscosity directly explains the observed change in $E_{a\text{-}cond}$ with DOS. Tests are being carried out to further elucidate the role of ionic mobility and edge effects at the pore wall on the $E_{a\text{-}cond}$.

3.7 Conclusions

The factors that affect $E_{a\text{-}cond}$ were studied on a range of concrete specimens and pore solutions. This was done in an effort to explain the wide range of reported $E_{a\text{-}cond}$ values reported in the literature (from 9 kJ/mol to 39 kJ/mol). Saturated specimens with an average $E_{a\text{-}cond}$ of 15.8 kJ/mol approached a theoretical minimum attainable activation energy represented by the $E_{a\text{-}cond}$ of the pore solutions (13.9 kJ/mol). $E_{a\text{-}cond}$ increases proportionally to a reduction in DOS. The trend was stronger for individual mixtures as compared to the trend when all measured specimens were considered. Behavior at low values of DOS is similar to that of a frozen specimen, where only a thin layer of fluid remains between the ice and pore wall. As such, a maximum achievable $E_{a\text{-}cond}$ is conceptually similar to the $E_{a\text{-}cond}$ of a specimen after freezing.

A change in the DOS affects the resistivity of the specimen by changing fluid filled porosity, concentration of ions in the pore solution, and the connectivity of the fluid filled pores – therefore, these are possible reasons that explain the effect of DOS on the $E_{a\text{-}cond}$. It was shown that changes in ionic concentration have little effect on $E_{a\text{-}cond}$. This was shown on several extracted pore solutions as well as on a wide range of simulated pore solutions.

The effects of $E_{a\text{-}cond}$ from a reduced moisture content were determined to be due to a change in the connectivity of the fluid filled pores (β'). This could be an ionic mobility effect due to an edge effect of the pore wall.

Ideally, being able to measure $E_{a\text{-}cond}$ for every concrete specimen or characterizing an $E_{a\text{-}cond}$ for a specific mixture at a specific moisture content would

produce the best results. This is however not always feasible especially in the case of modeling. If moisture content is known, a relation of $E_{a\text{-}cond} = 33.3 – 16.3 \cdot DOS$ may be used.

3.8 Future Work

There are aspects of this work that have yet to be explored to their fullest. Further progress may be made in the following areas:

- $E_{a\text{-}cond}$ was studied on a wide range of concrete paving mixtures from across the states containing various amounts of supplementary cementitious materials, however w/cm only ranged from 0.37 to 0.44. It would be interesting to see what effects a wide range of w/cm displays on the relationships of $E_{a\text{-}cond}$ against DOS and β'.
- $E_{a\text{-}cond}$ was found to be dependent of the fluid filled tortuosity of the specimen β'. It may be of interest to measure $E_{a\text{-}cond}$ of materials that have known and well defined microstructural properties. This may include siltstone or other porous rock that are used as embedded pore solution resistivity meters. In particular it would be interesting to study $E_{a\text{-}cond}$ with values of β' between 0.05 and 1.
- $E_{a\text{-}cond}$ was determined for specimens at moisture contents as low as 50% DOS. When at this DOS and when at a temperature of 5°C, the electrical resistivity was too high for the setup used in this study to measure and yielded an error reading. It may be possible to measure resistivity at a DOS lower than 50% if measuring at temperatures higher than what was prescribed in this

study. It would be interesting to see if the trend of $E_{a\text{-}cond}$ vs DOS remains linear throughout lower values of DOS. It would also be interesting to see if $E_{a\text{-}cond}$ at low DOS corresponds well with Ea-cond of a specimen that has undergone freezing.

- It was discussed that concrete specimens undergoing freezing experience a rapid increase in $E_{a\text{-}cond}$ corresponding to the rapid formation of ice and subsequent loss of conductive fluid. This observation is similar to the observed gradual increase of $E_{a\text{-}cond}$ as drying occurs and moisture content is reduced. An extension of this discussion could be to examine how $E_{a\text{-}cond}$ changes as it undergoes a well controlled thawing process.
- $E_{a\text{-}cond}$ was measured for different solutions with varied viscosities η. Although there was a clear correlation between the effects of temperature on both viscosity and electrical conduction, and the relation between ionic mobility and viscosity of solutions has been shown, it was unclear if viscosity contributes to the change in $E_{a\text{-}cond}$ seen with decreasing DOS.

3.9 Acknowledgments

This work was conducted as part of a multi-laboratory study with mixtures from the Performance Engineered Mixtures (PEM) Champion States and as part of the National Concrete Consortium. Experiments in this study were performed at Oregon State University at the Kiewit Materials Performance Lab and Concrete Performance Lab.

4. Conclusions

This thesis examined temperature corrections for resistivity measurements in concrete. It explored the hypothesis that an activation energy approach along with careful consideration of $E_{a\text{-}cond}$ values should be implemented as a standard way to correct for measuring resistivity of concrete specimens at different temperature. Such corrections can enable the accurate use of resistivity measurements in the determination of formation factor as using an incorrect temperature correction can produce significant errors. It is proposed that an activation energy based correction be used as opposed to a linear correction, and that care should be taken when choosing a value of $E_{a\text{-}cond}$.

The main conclusions from this study are:

- Predictions using an activation energy and a linear approach were linearly related and mathematically comparable at low temperature sensitivities ($E_{a\text{-}cond}$ of 0-15 kJ/mol). This range is comparable to values obtained for typical pore solutions. Predictions at higher temperature sensitivities ($E_{a\text{-}cond}$ of 15-45 kJ/mol) showed a nonlinear relation between using an activation energy and linear approach. These values correspond to a range of activation energies found in concrete specimens.
- An activation energy approach produced smaller errors than a linear approach when compared to measured data. This finding was more pronounced in sealed specimens.
- An equation is given to convert an α correction to an $E_{a\text{-}cond}$ correction if the testing temperatures of the specimens are known.

- $E_{a\text{-}cond}$ for concrete specimens was highly dependent on the moisture condition of the specimen. Extracted pore solutions typically have $E_{a\text{-}cond}$ values slightly lower than vacuum saturated specimens.
- The effect of moisture condition and degree of saturation on $E_{a\text{-}cond}$ was shown to not be an effect of dilution. Solutions of different ionic strength have similar $E_{a\text{-}cond}$ values. The effect of degree of saturation was due to a change in the connectivity of the fluid filled pores.
- Viscosity of a solution can greatly impact the $E_{a\text{-}cond}$ value.
- Pore solutions represent a minimum achievable $E_{a\text{-}cond}$ value for concrete specimens and the $E_{a\text{-}cond}$ of a frozen specimen represents a maximum achievable value.
- Saturated specimens have $E_{a\text{-}cond}$ of 15.8 kJ/mol with low COV (4.39%). Sealed specimens have $E_{a\text{-}cond}$ of 29.8 kJ/mol with a higher COV (8.21%) due to a wider range of degree of saturation. For extracted pore solutions, a $E_{a\text{-}cond}$ value of 13.9 kJ/mol was obtained.
- If the moisture content of the specimen is known, the equation $E_{a\text{-}cond} = 33.3 – 16.3 \cdot DOS$ may be used.

5. Bibliography

1. Shimizu, Y. An Electrical Method for Measuring the Setting Time of Portland Cement. *Mill Section of Concrete*, Vol. 32, No. 5, 1928, pp. 111–113.

2. Gu, P., P. Xie, J. J. Beaudoin, and R. Brousseau. A.C. Impedance Spectroscopy (I): A New Equivalent Circuit Model for Hydrated Portland Cement Paste. *Cement and Concrete Research*, Vol. 22, No. 5, 1992, pp. 833–840. https://doi.org/10.1016/0008-8846(92)90107-7.

3. Schiessel, A., W. J. Weiss, J. D. Shane, N. S. Berke, T. O. Mason, and S. P. Shah. Assessing the Moisture Profile of Drying Concrete Using Impedance Spectroscopy. *Concrete Science and Engineering*, Vol. 2, No. 6, 2000, pp. 106–116.

4. Andrade, M. C., F. Bolzoni, and J. Fullea. Analysis of the Relation between Water and Resistivity Isotherms in Concrete. *Materials and Corrosion*, Vol. 62, No. 2, 2011, pp. 130–138. https://doi.org/10.1002/maco.201005777.

5. Layssi, H., P. Ghods, A. R. Alizadeh, and M. Salehi. Electrical Resistivity of Concrete. *Concrete International*, Vol. 37, No. 5, 2015, pp. 41–46.

6. Rupnow, T., and P. Icenogle. Surface Resistivity Measurements Evaluated as Alternative to Rapid Chloride Permeability Test for Quality Assurance and Acceptance. *Transportation Research Record: Journal of the Transportation Research Board*, Vol. 2290, 2012, pp. 30–37. https://doi.org/10.3141/2290-04.

7. Spragg, R., C. Villani, and J. Weiss. Electrical Properties of Cementitious Systems: Formation Factor Determination and the Influence of Conditioning Procedures. *Advances in Civil Engineering Materials*, Vol. 5, No. 1, 2016, pp. 124–148. https://doi.org/10.1520/ACEM20150035.

8. Julio-Betancourt, G. A., and R. D. Hooton. Study of the Joule Effect on Rapid Chloride Permeability Values and Evaluation of Related Electrical Properties of Concretes. *Cement and Concrete Research*, Vol. 34, No. 6, 2004, pp. 1007–1015. https://doi.org/10.1016/j.cemconres.2003.11.012.

9. Whiting, D. Rapid Measurement of the Chloride Permeability of Concrete. *Public Roads*, Vol. 45, No. 3, 1981, pp. 101–112.

10. Whiting, D., and T. M. Mitchell. History of the Rapid Chloride Permeability Test. *Transportation Research Record*, Vol. 1335, No. 1, 1992, pp. 55–62.

11. SIMCO Technologies. *STADIUM LAB User Guide, V3.0*. 2011.

12. Nokken, M. R., and R. D. Hooton. Using Pore Parameters to Estimate Permeability or Conductivity of Concrete. *Materials and Structures*, Vol. 41, No. 1, 2007, pp. 1–16. https://doi.org/10.1617/s11527-006-9212-y.

13. Presuel-Moreno, F. J., Y. Liu, and A. Suares. Final Report: Characterization of New and Old Concrete Structures Using Surface Resistivity Measurements. 2010, p. 263.

14. Spragg, R., C. Villani, K. Snyder, D. Bentz, J. Bullard, and J. Weiss. Factors That Influence Electrical Resistivity Measurements in Cementitious Systems. *Transportation Research Record: Journal of the Transportation Research Board*, Vol. 2342, No. 2342, 2013, pp. 90–98. https://doi.org/10.3141/2342-11.

15. Poursaee, A., and W. J. Weiss. An Automated Electrical Monitoring System (AEMS) to Assess Property Development in Concrete. *Automation in Construction*, Vol. 19, No. 4, 2010, pp. 485–490. https://doi.org/10.1016/j.autcon.2009.12.016.

16. Rajabipour, F., and W. J. Weiss. *Parameters Affecting the Measurements of Embedded Electrical Sensors for Concrete Health Monitoring Applications*. 2008.

17. Morris, W., E. I. Moreno, and A. A. Sagüés. Practical Evaluation of Resistivity of Concrete in Test Cylinders Using a Wenner Array Probe. *Cement and Concrete Research*, Vol. 26, No. 12, 1996, pp. 1779–1787. https://doi.org/10.1016/S0008-8846(96)00175-5.

18. Spragg, R., Y. Bu, K. Snyder, D. P. Bentz, and J. Weiss. Electrical Testing of Cement-Based Materials: Role of Testing Techniques, Sample Conditioning, and Accelerated Curing. *Publication FHWA/IN/JTRP-2013/28. Joint Transportation Research Program*, 2013. https://doi.org/10.5703/1288284315230.

19. Snyder, K. A. The Relationship between the Formation Factor and the Diffusion Coefficient of Porous Materials Saturated with Concentrated Electrolytes: Theoretical and Experimental Considerations. *Concrete Science and Engineering*, Vol. 3, No. 12, 2001, pp. 216–224. https://doi.org/10.1017/CBO9781107415324.004.

20. Spragg, R. P., S. Z. Jones, Y. Bu, Y. Lu, D. P. Bentz, K. Snyder, and J. Weiss. Leaching of Conductive Species: Implications to Measurements of Electrical Resistivity. *Cement and Concrete Composites*, Vol. 79, 2017, pp. 94–105. https://doi.org/10.1016/j.cemconcomp.2017.02.003.

21. McCarter, W. J., and S. Garvin. Dependence of Electrical Impedance of Cement-Based Materials on Their Moisture Condition. *Journal of Physics D:*

Applied Physics, Vol. 22, No. 11, 2000, pp. 1773–1776. https://doi.org/10.1088/0022-3727/22/11/033.

22. Weiss, J., K. Snyder, J. Bullard, and D. P. Bentz. Using a Saturation Function to Interpret the Electrical Properties of Partially Saturated Concrete. *Journal of Materials in Civil Engineering*, Vol. 25, No. 8, 2013, pp. 1097–1106. https://doi.org/10.1061/(ASCE)MT.1943-5533.0000549.

23. McCarter, W. J., M. C. Forde, and H. W. Whittington. Resistivity Characteristics of Concrete. *Institution of Civil Engineers Proceedings*, Vol. 71, No. 1, 1981, pp. 107–117. https://doi.org/10.1680/iicep.1982.1993.

24. McCarter, W. J. Effects of Temperature on Conduction and Polarization in Portland Cement Mortar. *Journal of the American Ceramic Society*, Vol. 78, No. 2, 1995, pp. 411–415. https://doi.org/10.1111/j.1151-2916.1995.tb08816.x.

25. Elkey, W., and E. J. Sellevold. Electrical Resistivity of Concrete. *Norwegian Road Research Laboratory Publication no.80*, 1995, pp. 1–36.

26. Tumidajski, P. J., A. S. Schumacher, S. Perron, P. Gu, and J. J. Beaudoin. On the Relationship between Porosity and Electrical Resistivity in Cementitious Systems. *Cement and Concrete Research*, Vol. 26, No. 4, 1996, pp. 539–544. https://doi.org/10.1016/0008-8846(96)00017-8.

27. Archie, G. E. The Electrical Resistivity Log as an Aid in Determining Some Reservoir Characteristics. *Transactions of the AIME*, Vol. 146, No. 01, 1942, pp. 54–62. https://doi.org/10.2118/942054-G.

28. Christensen, B. J., T. Coverdale, R. A. Olson, S. J. Ford, E. J. Garboczi, H. M. Jennings, and T. O. Mason. Impedance Spectroscopy of Hydrating Cement Based Materials: Measurement, Interpretation, and Application. *Journal of the American Ceramic Society*, Vol. 77, No. 11, 1994, pp. 2789–2804. https://doi.org/10.1111/j.1151-2916.1994.tb04507.x.

29. Weiss, W. J., T. J. Barrett, C. Qiao, and H. Todak. Toward a Specification for Transport Properties of Concrete Based on the Formation Factor of a Sealed Specimen. *Advances in Civil Engineering Materials*, Vol. 5, No. 1, 2016, pp. 179–194. https://doi.org/10.1520/ACEM20160004.

30. Snyder, K. A., X. Feng, B. D. Keen, and T. O. Mason. Estimating the Electrical Conductivity of Cement Paste Pore Solutions from OH- , K+ and Na+ Concentrations. No. 6, 2003, pp. 793–798.

31. Barneyback, R. S., and S. Diamond. Expression and Analysis of Pore Fluids From Hardened Pastes and Mortars. *Cement and Concrete Research*, Vol. 11, 1981, pp. 279–285.

32. Spragg, R., C. Qiao, T. Barrett, and J. Weiss. Assessing a Concrete's Resistance to Chloride Ion Ingress Using the Formation Factor. In *Corrosion of Steel in Concrete Structures*, pp. 211–238.

33. Barrett, T. J. *Improving Service Life of Concrete Structures Through the Use of Internal Curing: Impact on Practice*. Phd. Thesis Purdue University, 2015.

34. Chrisp, T. M., G. Starrs, W. J. McCarter, E. Rouchotas, and J. Blewett. Temperature-Conductivity Relationships for Concrete: An Activation Energy Approach. *Journal of Materials Science Letters*, Vol. 20, No. 12, 2001, pp. 1085–1087. https://doi.org/10.1023/A:1010926426753.

35. Sant, G., F. Rajabipour, and W. J. Weiss. The Influence of Temperature on Electrical Conductivity Measurements and Maturity Predictions in Cementitious Materials During Hydration. *Indian Concrete Journal*, Vol. 82, 2008, pp. 7–16.

36. Castro, J., R. Spragg, P. Compare, W. J. Weiss, P. Kompare, and W. J. Weiss. Portland Cement Concrete Pavement Permeability Performance. *Publication FHWA/IN/JTRP-2010/29. Joint Transportation Research Program*, 2010. https://doi.org/10.5703/1288284314244.

37. Polder, R. B. Test Methods for on Site Measurement of Resistivity of Concrete - A RILEM TC-154 Technical Recommendation. *Construction and Building Materials*, Vol. 15, No. 2-3, 2001, pp. 125–131. https://doi.org/10.1016/S0950-0618(00)00061-1.

38. Rupnow, T., and P. Icenogle. Development of a Precision Statement for Concrete Surface Resistivity. *Transportation Research Record: Journal of the Transportation Research Board*, Vol. 2290, 2011, pp. 38–43. https://doi.org/10.3141/2290-05.

39. Ma, H., D. Hou, and Z. Li. Two-Scale Modeling of Transport Properties of Cement Paste: Formation Factor, Electrical Conductivity and Chloride Diffusivity. *Computational Materials Science*, Vol. 110, 2015, pp. 270–280. https://doi.org/10.1016/j.commatsci.2015.08.048.

40. Rajabipour, F., and J. Weiss. Linking Health Monitoring in Concrete Structures with Durability Performance Simulations. *Structures Congress 2006*, 2006, pp. 1–10. https://doi.org/10.1061/40889(201)97.

41. Chrisp, T. M., W. J. McCarter, G. Starrs, and J. Blewett. Field Trials on Covercrete Monitoring Sensors: A Temperature Correction Protocol for Conductivity Measurements. *Innovations and Developments in Concrete Materials and Construction*, Vol. 1, 2002, pp. 325–335.

42. Hammond, E., and T. Robson. Comparison of Electrical Properties of Various Cements and Concretes. *The Engineer*, Vol. 199, 1955, pp. 78–80.

43. Rajabipour, F., and J. Weiss. Electrical Conductivity of Drying Cement Paste. *Materials and Structures*, Vol. 40, 2007, pp. 1143–1160. https://doi.org/10.1617/s11527-006-9211-z.

44. Bu, Y., and J. Weiss. The Influence of Alkali Content on the Electrical Resistivity and Transport Properties of Cementitious Materials. *Cement and Concrete Composites*, Vol. 51, 2014, pp. 49–58. https://doi.org/10.1016/j.cemconcomp.2014.02.008.

45. ASTM C595/C595M-16. Standard Specification for Blended Hydraulic Cements. *ASTM International*, 2016, pp. 1–13. https://doi.org/10.1520/C0595.

46. Farnam, Y., H. Todak, R. Spragg, and J. Weiss. Electrical Response of Mortar with Different Degrees of Saturation and Deicing Salt Solutions during Freezing and Thawing. *Cement and Concrete Composites*, Vol. 59, 2015, pp. 49–59. https://doi.org/10.1016/j.cemconcomp.2015.03.003.

47. Weiss, J., J. D. Shane, A. Mieses, T. O. Mason, and S. P. Shah. Aspects of Monitoring Moisture Changes Using Electrical Impedance Spectroscopy. *Proceedings of the second international Research Seminar in Lund*, 1999, pp. 31–48.

48. Spragg, R. P., J. Castro, T. Nantung, M. Paredes, and J. Weiss. Variability Analysis of the Bulk Resistivity Measured Using Concrete Cylinders. *Advances in Civil Engineering Materials*, Vol. 1, No. 1, 2012, pp. 1–16. https://doi.org/10.1520/ACEM104596.

49. Bu, Y., R. Spragg, and W. J. Weiss. Comparison of the Pore Volume in Concrete as Determined Using ASTM C642 and Vacuum Saturation. *Advances in Civil Engineering Materials*, Vol. 3, No. 1, 2014, pp. 308–315. https://doi.org/10.1520/ACEM20130090.

50. Whittington, H. W., J. McCarter, and M. C. Forde. The Conduction of Electricity Through Concrete. *Magazine of Concrete Research*, Vol. 33, No. 114, 1981, pp. 48–60.

51. Mettler Toledo. Reducing Common Errors in Conductivity Measurements. *Mettler Toledo*. 1–6. http://www.mt.com/dam/MT NA/pHCareCenter/Conductivity_Reduce_Common_Errors_WP.pdf. Accessed Jul. 10, 2017.

52. Mettler Toledo. Conductivity Measurement: Linear Temperature Compensation. *Mettler Toledo*. 1–2. http://www.mt.com/dam/MT

NA/pHCareCenter/Conductivity_Linear_Temp_Comensation_APN.pdf . Accessed Jul. 10, 2017.

53. Barron, J. J., and C. Ashton. The Effect of Temperature on Conductivity Measurement. *TSP*, Vol. 7, No. 3, 2005, pp. 1–5.

54. Light, T. S. Temperature Dependence and Measurement of Resistivity of Pure Water. *Analytical Chemistry*, Vol. 56, 1984, pp. 1138–1142. https://doi.org/10.1021/ac00271a019.

55. McCarter, W. J., G. Starrs, and T. M. Chrisp. Electrical Conductivity, Diffusion, and Permeability of Portland Cement-Based Mortars. *Cement and Concrete Research*, Vol. 30, No. 9, 2000, pp. 1395–1400. https://doi.org/10.1016/S0008-8846(00)00281-7.

56. Coyle, A., R. Spragg, A. Amirkhanian, P. Suraneni, and J. Weiss. Comparison of Linear Temperature Corrections and Activation Energy Temperature Corrections for Electrical Resistivity of Concrete. *Transportation Research Board - Submitted*, 2017.

57. McCarter, W. J., G. Starrs, T. M. Chrisp, P. a M. Basheer, S. V. Nanukuttan, and S. Srinivasan. Conductivity/Activation Energy Relationships for Cement-Based Materials Undergoing Cyclic Thermal Excursions. *Journal of Materials Science*, Vol. 50, No. 3, 2015, pp. 1129–1140. https://doi.org/10.1007/s10853-014-8669-2.

58. Rajabipour, F. *Fundamental Investigations on Utilizing Electrical Sensing to Improve Life Cycle Modeling of Concrete Structures*. M.S. Thesis Purdue University, 2003.

59. Chang, M. T., P. Suraneni, O. B. Isgor, D. Trejo, and W. J. Weiss. Using X-Ray Fluorescence to Assess the Chemical Composition and Resistivity of Simulated Cementitious Pore Solutions. *International Journal of Advances in Engineering Sciences and Applied Mathematics*, 2017, pp. 1–8. https://doi.org/10.1007/s12572-017-0181-x.

60. Rajabipour, F., G. Sant, and J. Weiss. Development of Electrical Conductivity-Based Sensors for Health Monitoring of Concrete Materials. *Transportation Research Board*, 2007, pp. 1–16.

61. Andrade, E. N. A Theory of the Viscosity of Liquids.—Part I. *The London, Edinburgh, and Dublin Philosophical Magazine and Journal of Science*, Vol. 17, No. 112, 1934, pp. 495–511.

62. Chen, Y. M., and A. J. Pearlstein. Viscosity-Temperature Correlation for Glycerol-Water Solutions. *Industrial & Engineering Chemistry Research*, Vol. 26, No. 8, 1987, pp. 1670–1672. https://doi.org/10.1021/ie00068a030.

63. Westbrook, C. Calculate Density and Viscosity of Glycerol/water Mixtures. http://www.met.reading.ac.uk/~sws04cdw/viscosity_calc.html. Accessed Sep. 19, 2017.

64. Cheng, N. Formula for the Viscosity of a Glycerol-Water Mixture. *Industrial & Engineering Chemistry Research*, Vol. 47, No. 9, 2008, pp. 3285–3288.

65. Bourne, J. R., P. Dell'Ava, O. Dossenbach, and T. Post. Densities, Viscosities, and Diffusivities in Aqueous Sodium Hydroxide-Potassium Ferri- and Ferrocyanide Solutions. *Journal of Chemical and Engineering Data*, Vol. 30, No. 2, 1985, pp. 160–163. https://doi.org/10.1021/je00040a008.